JPL Publication 15-7

The JPL Uranian Radiation Model (UMOD)

Henry Garrett
Luz Maria Martinez-Sierra
Jet Propulsion Laboratory

Robin Evans
Mori Associates, Inc.
Rockville, Maryland

National Aeronautics and Space Administration

Jet Propulsion Laboratory
California Institute of Technology
Pasadena, California

September 2015

This research was carried out at the Jet Propulsion Laboratory, California Institute of Technology, under a contract with the National Aeronautics and Space Administration.

Acknowledgments

The authors would like to thank M. Boyles for his interest in funding and having the UMOD radiation model made available for general JPL use. Finally I. Jun and W. Kim as always have provided important and critical feedback on the model and its applications.

Table of Contents

Figures

Tables

Abstract

The objective of this study is the development of a comprehensive radiation model (UMOD) of the Uranian environment for JPL mission planning. The ultimate goal is to provide a description of the high energy electron and proton environments and the magnetic field at Uranus that can be used for engineering design. Currently no model exists at JPL. A preliminary electron radiation model employing Voyager 2 data was developed by Selesnick and Stone in 1991. The JPL Uranian Radiation Model extends that analysis, which modeled electrons between 0.7 MeV and 2.5 MeV based on the Voyager Cosmic Ray Subsystem electron telescope, down to an energy of 0.022 MeV for electrons and from 0.028 MeV to 3.5 MeV for protons. These latter energy ranges are based on measurements by the Applied Physics Laboratory Low Energy Charged Particle Detector on Voyager 2. As in previous JPL radiation models, the form of the Uranian model is based on magnetic field coordinates and requires a conversion from spacecraft coordinates to Uranian-centered magnetic "B-L" coordinates. Two magnetic field models have been developed for Uranus: 1) a simple "offset, tilted dipole" (OTD), and 2) a complex, multi-pole expansion model ("Q_3"). A review of the existing data on Uranus and a search of the NASA Planetary Data System (PDS) were completed to obtain the latest, up to date descriptions of the Uranian high energy particle environment. These data were fit in terms of the Q_3 B-L coordinates to extend and update the original Selesnick and Stone electron model in energy and to develop the companion proton flux model. The flux predictions of the new model were used to estimate the total ionizing dose for the Voyager 2 flyby, and a movie illustrating the complex radiation belt variations was produced to document the uses of the model for planning purposes.

1. Introduction

Figure 1 is a high resolution image showing faint cloud features on Uranus and its rings (Keck Observatory, 2007). As noted in the last Planetary Decadal Survey (*Vision and Voyages for Planetary Science in the Decade 2013-2022;* National Academy of Sciences, 2011) by the National Research Council, Uranus, the next giant planet after Jupiter and Saturn, differs dramatically from them and is "a wholly distinct class of planet." As illustrated in Fig. 2, because of its highly inclined spin axis and tilt of its magnetic field, Uranus has a unique magnetospheric configuration and interaction with the Solar Wind. As a result, a Uranus Orbiter and Probe Flagship Mission to explore the planet, its atmosphere, rings, and moons has been listed as the third priority in the *Planetary Decadal Survey*. To design a successful spacecraft mission, detailed knowledge of the Uranian environment, particularly its magnetic field and radiation belts, is required to determine the required radiation shielding.

Voyager 2 flew within 107,000 km of Uranus on January 24, 1986. During this flyby, several instruments on board measured the trapped radiation at Uranus. This radiation environment, while relatively mild compared to that at the Earth, Saturn, and Jupiter, represents a basically unknown potential threat to future missions to Uranus. The purpose of this study is to revisit the original analyses of the Voyager team (Mauk et al., 1987; Selesnick and Stone, 1991; Connerney et al., 1987) and, based on published findings, provide a simple computer model for the Uranian radiation environment that can be used for mission planning. As mentioned, Uranus has been proposed as a potential outer planets target, and several recent Uranus mission studies have been

completed at JPL and other centers—but without any consideration of the radiation environment. Uranus, because of its tilted magnetic field (almost 60 degrees, deg) to the spin axis) and its inclined spin axis (~98 deg), (see Fig. 2) represents a challenge compared to previous radiation belt models. To develop a working model of this complex environment requires both a model of the electron and proton particle fluxes versus pitch angle and energy. These are usually given in terms of magnetic field coordinates (B-L). Spacecraft location in a Uranian-centric system must then be transformed into B-L coordinates. Once the position of the spacecraft in magnetic coordinates is determined, the particle fluxes are then fit as functions of energy, pitch angle, and B-L. The details of these fitting processes, a review of the data, and a description of the final Uranus radiation model FORTRAN code, UMOD, for simulating the Uranian environment are presented in the following.

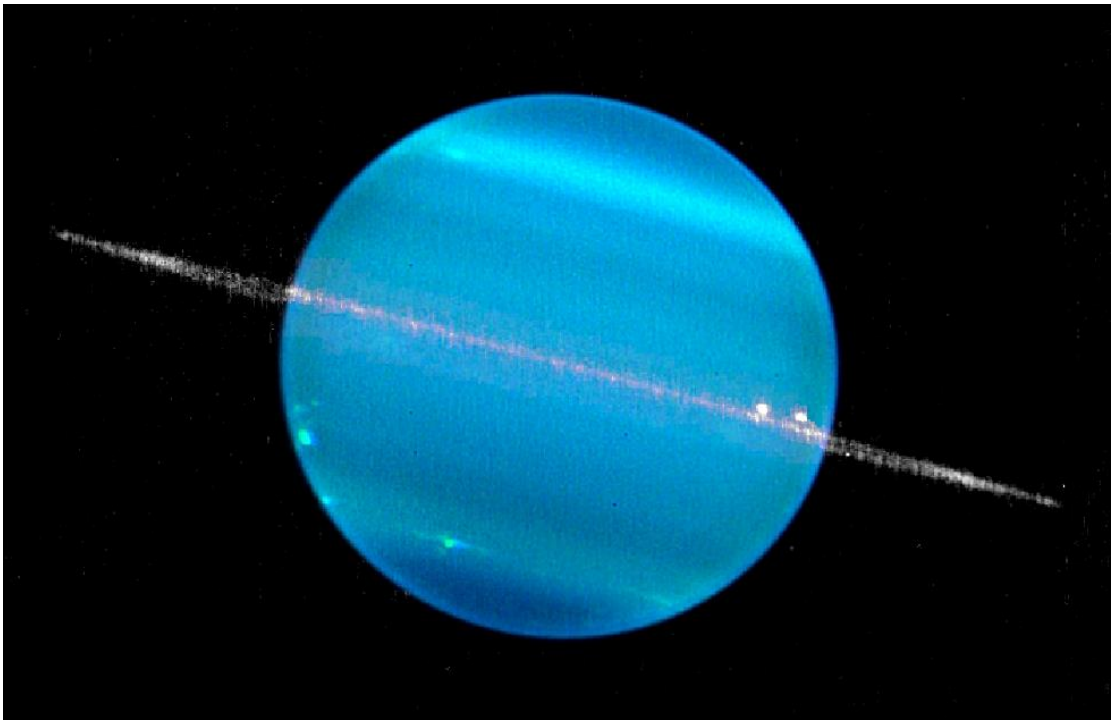

Figure 1. Keck II composite image of Uranus.

The image is comprised of two different infrared wavelengths with Uranus appearing brighter in the H-band filter while the rings appear enhanced in the K-band filter. The image shows subtle cloud features and the equatorial ring surrounding Uranus. Credit: W. M. Keck Observatory, Mauna Kea Access Rd, Hawaii (Marcos van Dam), May 28, 2007 (http://www.keckobservatory.org/recent/entry/scientists_study_changes_in_planets_rings).

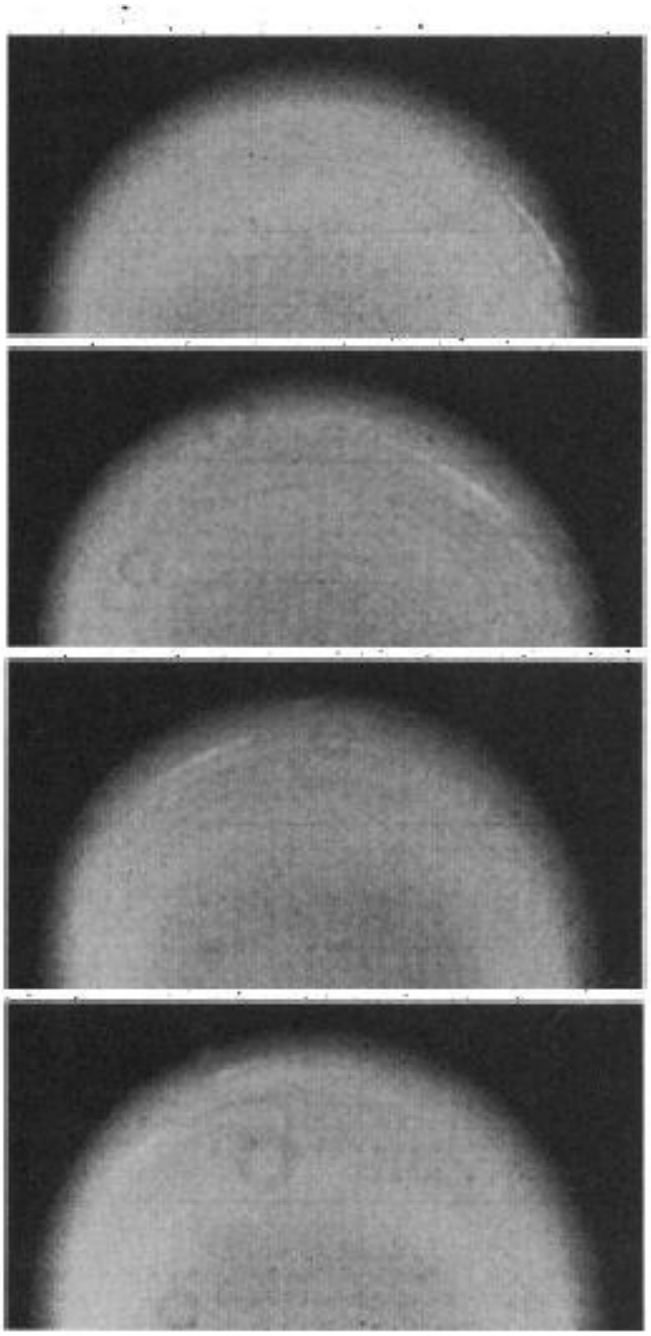

Figure 2. Time lapse sequence of four narrow-angle orange filter images showing small-scale bands and discrete features at latitudes from –25 to –40 deg. The counterclockwise rotation is clearly visible in this 4.6-hour sequence.
(http://www.jpl.nasa.gov/spaceimages/details.php?id=PIA00369; also, Smith et al, 1986)

2. Planetary Data System (PDS) and Modern Uranus Coordinates

The first step in analyzing the Uranian data is to establish as accurately as possible the location of Voyager relative to Uranus. In generating the position data for Voyager 2 and modeling the Uranian magnetic field, a major difficulty is the uncertainty in a very basic quantity—the planetary rotation rate. Referring back to the original Uranian flyby, the planetary encounter by Voyager was preceded by a flurry of ground-based observations before the flyby. These observations were both to help the in-situ science observation of Voyager and as a last chance to make meaningful observations before the Voyagers had the final word or until other flybys or orbiters reached the planet. Following the flyby there was a period of approximately 2 years of detailed analyses and publishing of the Voyager findings. After that there was a big decrease in ground-based observations because they could not compete with the in-situ observations. In the case of Uranus, some of the Voyager observations have taken a very long time to get "in the textbooks." Thus, any analysis of the Voyager Uranus data entails some "forensic" investigation to set the stage for further studies. In the process of performing that study, Evans found that the definition of the Uranian coordinate system at the time of the fly-by was very different from that currently used by the JPL Spacecraft Planets Instrument C-Matrix Events SPICE system (the SPICE ancillary information system, part of NASA's Navigation and Ancillary Information Facility (NAIF), is used to compute the trajectories and other geometric information used in analyzing science observations). To adequately address this issue, a detailed discussion is necessary of the steps performed in regenerating the PDS coordinates used by the original Voyager investigators from the SPICE coordinates.

See the PDS.nasa.gov website to access the various files.

3. Rotation Rate

The Uranus rotation rate before the Voyager 2 flyby in January 1986 was not well defined. Spectroscopic observations placed the rotation period between 12 and 24 hours, and dynamical flattening placed it in a narrower range of 15 to 17 hours. Desch et al. (1986) used Voyager radio and magnetospheric observations of 42 rotations to pin the rotation rate to 17.24 ±0.01 hour. JPL's SPICE routines, which did not exist until after the encounter, used an initial value of 15.57 hours before 1990. In 1990, SPICE adopted the "newer" value of 17.24 hours. Modern SPICE kernels are made from a fit to the original radio position data from Voyager using this newer value of the rotation rate. Figure 2 illustrates the rotation as seen in a set of Voyager images of clouds on Uranus. As shown, the pole was pointed almost directly at the Sun during the encounter. The rotation is counterclockwise about the sunlit pole.

SPICE assumes that the South Pole of Uranus is pointed toward the Sun in 1986 and that the rotation of the planet is retrograde. This is in accordance with the International Astronomical Union (IAU) definition that the North Pole of a planet or satellite shall be the pole which points above the invariable plane of the Solar System. The invariable plane is the plane perpendicular to the total Solar System angular momentum vector and passes through the Solar System barycenter. Leading to some confusion, there is an alternate definition that uses the right hand rule—that is, placing the right hand palm down on the Equator with the fingers pointing in the direction of rotation leaves the thumb pointing in the direction of the North Pole. This implies that the North Pole was pointed towards the Sun in 1986 and that the planet rotates prograde. The archived PDS data used this system.

The PDS archived position data can be reproduced from the SPICE files using a 15.57-hours prograde rotation rate and a Sun-pointed North Pole. There is, however, a problem with the labeling of West longitude (which this study traditionally terms "WLONG"). This study's interpretation of West longitude is: 360 deg – [PDS West longitude] = WLONG. If the PDS West longitude is used as defined, Connerney's Uranian magnetic field models cannot reproduce the published magnetic field plots or the actual PDS magnetic field data. The confusion comes from the PDS data label file which specifically states that the data are for "West longitude." The PDS COORDS.CAT file (the PDS catalog file explaining the format of the data) states that:

> *"Planetary longitudes are based on a 17.24 hour rotation period (Connerney et al., 1987) adopted by the Voyager Project shortly after the encounter. The zero longitude is defined by the requirement that the West Longitude of the spacecraft at 1800 SCET (spacecraft event time) day 24 (near closest approach) be 302 degrees West. Longitudes (WLONG) of the Uranus Longitude System (U1) are simply related to the angle PHI: WLONG = 360. - PHI (degrees)."*

The companion PDS file, POSDATA.FMT, states that the data are for longitude (it does not specify east or west). The data provided are most likely for the variable PHI (East Longitude) not West Longitude as implied above. The data in the file indicate that, at 18:00 on day 24, longitude = 58.25 deg, not 302 deg as stated in the COORDS.CAT file. Also note that PDS file states that the rotation period is 17.24 hour—this is most likely incorrect. The data and SPICE agree over the 20-hour flyby only if a 15.57-hour rotation rate is utilized. During the 20 hours of the PDS data (and SPICE with old rotation rate) the spacecraft changes its longitude by 664 deg. With SPICE and the 17.24-hour rotation rate the spacecraft changes by only 617 deg in the same period. The difference is the same as the difference in the rotation of the planet for the two

periods over 20 hours, or 47 deg. The 15.57-hour rotation period is a pre-Voyager estimate and appears to have been used in generating the original PDS data base.

4. Coordinates

To make the current SPICE coordinates (e.g., the coordinates that JPL would say were the actual Voyager coordinates as of today during the encounters) agree with the PDS, a SPICE file was modified to convert from modern SPICE to the PDS Voyager coordinates. SPICE file pck00003.tpc, the oldest existing SPICE planetary constants file for Uranus, has the lines:

```
BODY799_POLE_RA    = (  257.43     0.              0.  )
BODY799_POLE_DEC   = (  -15.10     0.              0.  )
BODY799_PM         = (  203.81  -501.1600928  0.  )
```

The first two lines give the North Pole axis direction pointing at right ascension (RA) = 257.43° and Declination (DEC) = -15.10 deg. Together, these are referred to as the North Pole position angle (NPPA). The third line states that the West longitude coordinates of the point on the planet below a stationary observer changes by: West Longitude = 203.81 - 501.1600928 * (days since J2000). (J2000 is the international standard for starting time referencing noon, Jan. 1, 2000 (Aoki, et al., 1983)). Here the 203.81 is the West Longitude that lines up with inertial coordinates at epoch J2000. 501.1600928 is the rotation rate in degrees per 24 hour day corresponding to the 17.24 hour rotation period. The (-) means retrograde rotation. The file, pck00003.tpc, states that it changed the rotation rate from pck00002.tpc from -554.913 deg per day (15.57-hour rotation period) to -501.1600928 degrees per day (17.24 hour rotation period). It changed only the one line (note change in first value to preserve the original J2000 longitudes on the planet):

```
BODY799_PM         = (  261.62  -554.913  0.  )
```

This file was dated June 25, 1990. The file pck00002.tpc is not available so, to make the SPICE results agree with the original PDS coordinates, the lines were modified to read:

```
BODY799_POLE_RA    = (  77.43          0.          0.  )
BODY799_POLE_DEC   = (  +15.10         0.          0.  )
BODY799_PM         = (  99.088584   554.913       0.  )
```

The first two lines reverse which pole is Sun-pointing (now North Pole), and the third line changes the sign and magnitude of the rotation (now prograde). It is not clear that 99.088584 keeps the J2000 West Longitude constant, but it just makes the coordinates line up with the PDS's requirement that the Voyager position be 302 deg West Longitude on Jan 24, 1986, at 18:00:00 (preserving a retrograde J2000 coordinate for a prograde rotation is probably incorrect anyway). The "corrected" pck file was named "pckURANUS_OLD_302.tpc" to differentiate it from other versions and prevent it from being used for any other purpose except to reproduce the "original" PDS coordinates. Use of this file reproduces the PDS positions with PDS West Longitude correctly delegated to East Longitude (i.e, it produces [360-PDS longitude] as WLONG).

Note: since 2004 the first two lines (NPPA) have changed slightly in the SPICE kernel to

```
BODY799_POLE_RA     = (  257.311    0.    0.   )
BODY799_POLE_DEC    = (  -15.175    0.    0.   )
```

This is a change made by the International Astronomical Union (IAU) in 1994, about the time the PDS data was published. As this unfortunately shows, things keep changing. Table 1 lists values for some of the constants used for Uranus. Along with the table, spin rates of ± 554.913 and ± 501.1600928 deg per 24-hour period were also used. We recommend using the values in red. Values were mixed and matched and not always in a consistent fashion in the literature.

Table 1. Voyager-derived and post-Voyager constants assumed for the Uranian system.

J2000	North Pole Right Ascension (deg)	Declination of North Pole (deg)	Polar Tilt (deg)
North Pole of invariable plane	273.8527	66.9911	
Uranus North Pole points away from Sun in 1986	77.311	15.175	96.93185
Uranus North Pole points towards from Sun in 1986	257.311	-15.175	83.06815
Uranus North Pole points away from Sun in 1986	77.43	15.1	97.01921
Uranus North Pole points towards from Sun in 1986	257.43	-15.1	82.98079
North Pole of orbit from ecliptic			0.772
North Pole of orbit from invariable plane			1.02
North Pole of ecliptic from invariable plane	270	66.560708	1.578725

Figure 3 shows the difference in SPICE and PDS East Longitudes using the above corrections. The peak difference is 0.72° with a root mean square (RMS) difference of 0.32°deg. Using the modern SPICE values for the pole-pointing vector gives an absolute and RMS error of 0.838 deg and 0.27 deg, respectively. Figures 4 and 5 give the differences in range and latitude between SPICE and the PDS. The range offset has an RMS of 0.035 R_U, and the latitude offset has an RMS of 0.27 deg. Note that the range data and SPICE predictions have small differences—the largest is 0.0669 R_U (1700 km) at a range of 24 R_U. This is reduced to ~0 km at closest approach and increases again after closest approach. Latitude differences peak at closest approach, and longitude differences peak about 3 hours after closest approach. Latitude and longitude differences are also small, on the order of 0.5 deg.

The "bad" point # 2 in the range plot is because PDS data for points #1 and #2 are identical, point #2 presumably being the bad point. The "bad" point at #582 in the range plot is incorrect. The break in range and longitude fits at #1342 is just a discontinuity in the time step (not visible in latitude because the line is horizontal there).

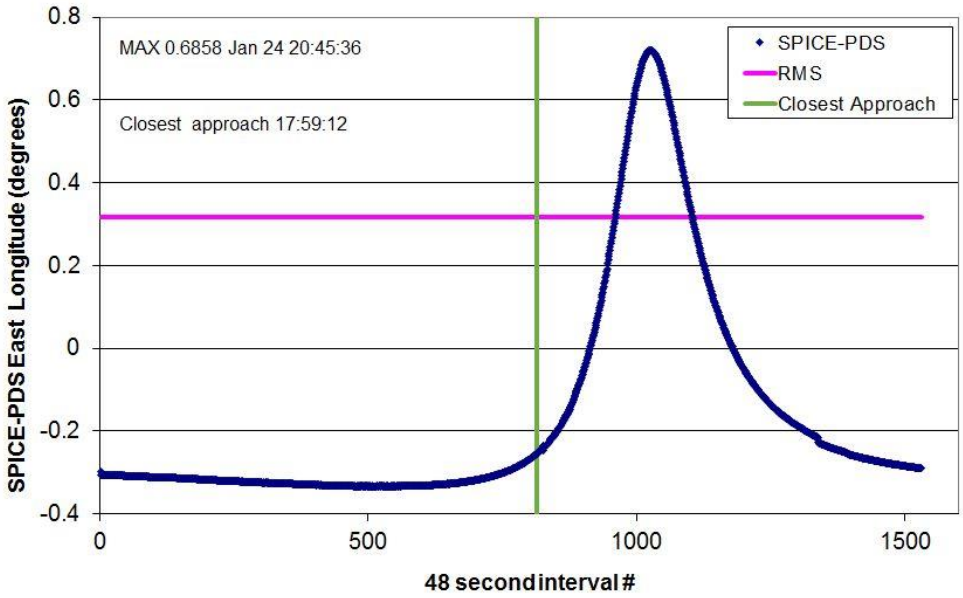

Figure 3. Offset of SPICE and PDS in east longitude using the RA = 77.43, Dec = 15.1 pole pointing vector and 554.913 deg per day rotation rate. Units are in degrees.

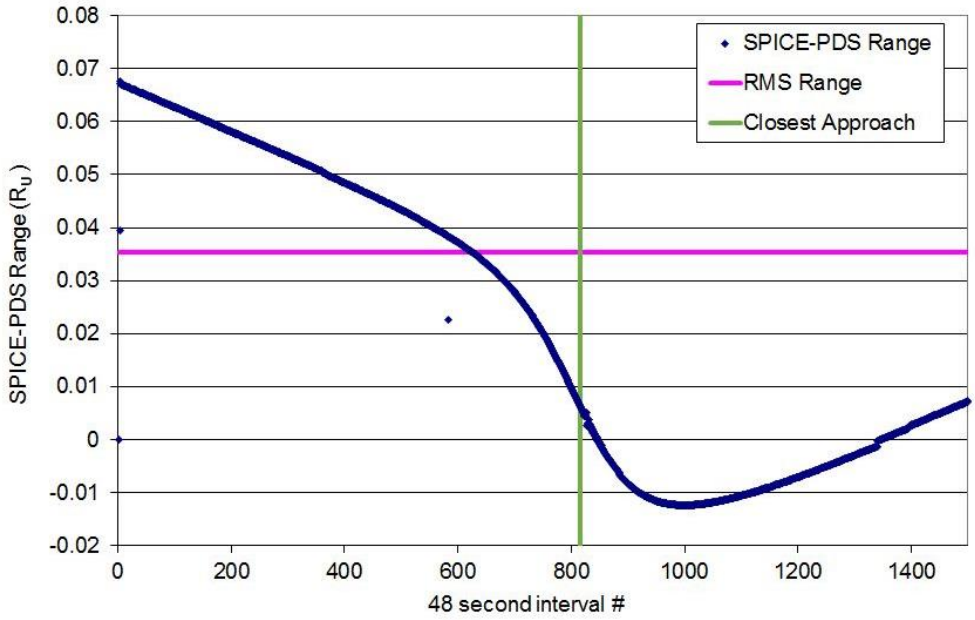

Figure 4. Offset of SPICE and PDS in range using the RA = 77.43, Dec = 15.1 pole pointing vector and 554.913 deg per day rotation rate. Units are in R_U.

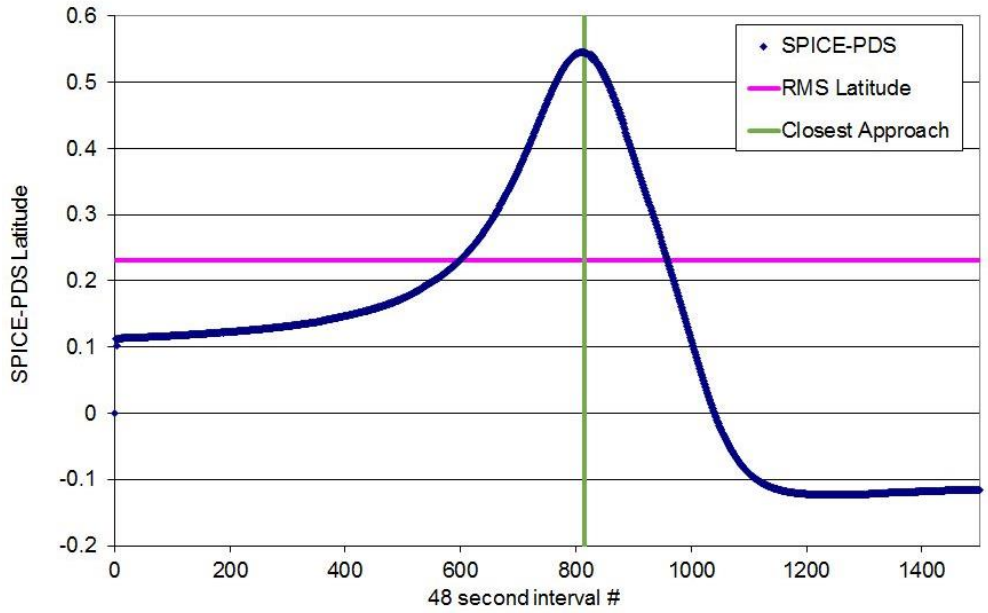

Figure 5. Offset of SPICE and PDS in latitude using the RA = 77.43, DEC = 15.1 pole pointing vector and 554.913 deg per day rotation rate. Units are in degrees.

The offsets in position between SPICE and the PDS look like a difference in coordinates between the two systems even after the above corrections are made. An attempt was made to minimize these by moving the pole. This was successful for longitude but did not affect the latitude (moving the pole location does not affect the range). The resulting "optimized" pole location was at RA 77.21 deg and DEC 15.03 deg. These are not recognized as published numbers so they will not be used. The plot of minimized differences is interesting in itself as it magnifies small errors in the data. Figure 6 is the minimized east longitude plot. Note that around closest approach, the Voyager track becomes double, and at closest approach there is a set of points in a vertical line. These might be digitizing errors or might be a result of the data link to Voyager being very noisy (assuming the range data are from fitting Doppler shifts).

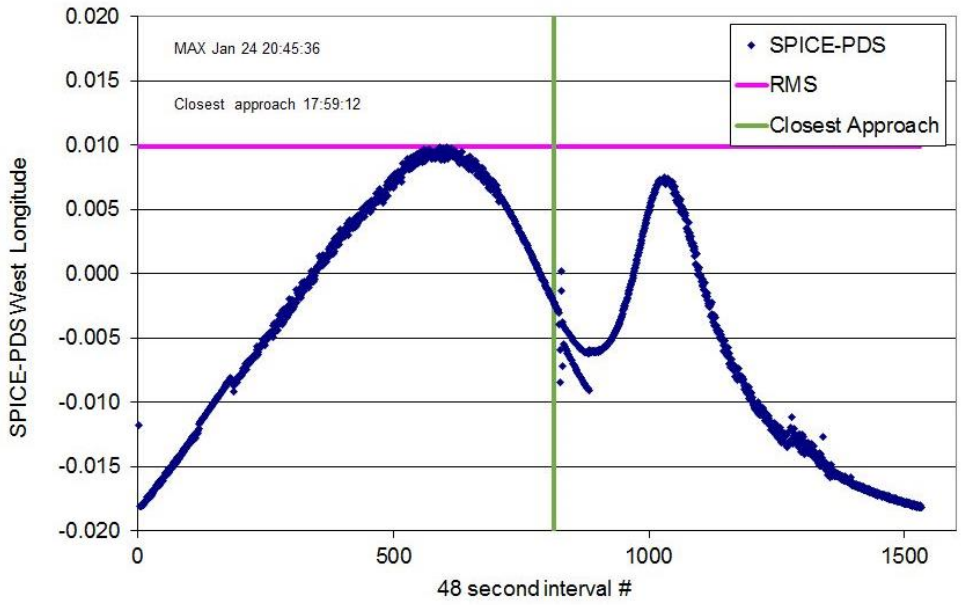

Figure 6. Reduced differences in the east longitude produced by shifting the pole location on Uranus (used only to show small errors in the data).

To validate these assumptions, the published magnetic field data were compared with the model predictions. In the literature, magnetic field models of both Ness et al. (1986) and Connerney et al. (1987) have been used to analyze the particle data. Ness et al. (1986) used a rotation rate of 17.29 hours (note: this is still another value for the rotation rate) and developed the offset tilted dipole model. Ness et al. (1986) and Connerney et al. (1987) both used 302.0 deg as the Voyager West Longitude on Jan. 24, 1986, at 18:00:00. They also adopted the PDS convention that the North Pole of Uranus was pointed towards the Sun in 1986 implying that this is the correct coordinate offset and orientation to use with the magnetic field models as provided in the open literature. Figure 7 shows the results of fitting the Uranian magnetic field along the Voyager 2 trajectory (see following section for discussion of Uranian magnetic field models). The first line (black) is for the original PDS magnetometer data and as illustrated in Fig. 2 of Connerney et al. (1987). The second line (green) is for the Q_3 model calculated using coordinates produced by the modified SPICE file, pckURANUS_OLD_mod.tpc. It overlies the PDS data in the region that was used for producing the model. The third line (blue) is the Q_3 model calculated using the PDS position data assuming that the PDS West longitude is "WLONG" as JPL defines it — it does not match the PDS data. The fourth line (red) is the Q_3 model calculated using the PDS position data assuming that the PDS West longitude is mislabeled and is really East Longitude. It also matches the PDS observations from day 24.42 to day 24.95 and closely overlays the SPICE-predicted Q_3 magnetic field values. The region used to fit the parameters for the Q_3 model is shown as the fifth line (purple). It is defined for $R_U \leq 8$.

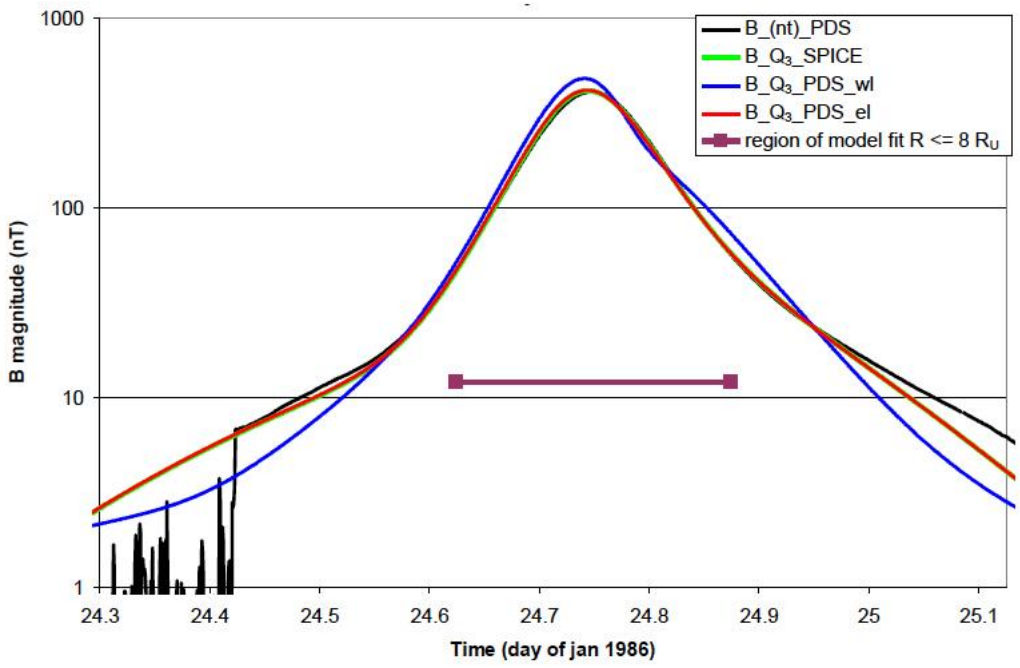

Figure 7. Magnetic field (B) values for various assumptions of the Uranus coordinates.

To summarize, it has been more than 26 years since Voyager 2 flew by Uranus. During that time, our understanding of the planet has changed dramatically. Indeed, the rotation rate, the location of the spin axis, and the definition of the "North/South" have changed, making it difficult to reproduce the PDS coordinates from the current JPL SPICE files. The PDS data can be understood, however, if we assume that the PDS longitude data (which were labeled at West Longitude) are assumed to be East Longitude. With that assumption, SPICE can then be modified to provide a correct plano-centric trajectory that will match the PDS coordinates. Future missions can then utilize mission trajectories produced by SPICE in an appropriate coordinate system (or as adapted from the official IAU coordinate conventions) to provide estimates of the magnetic field and radiation environment at Uranus using models based on the PDS data.

5. Uranian Magnetic Field

The first step in developing the Uranian radiation model is to provide a model of the magnetic field and the transformations necessary to compute the B and L coordinates of a point. The magnetic field of Uranus as measured by Voyager 2 is very distorted because it is offset and tilted ~60 deg to the Uranian spin axis. Figure 8 is a cross-section of the magnetic field (Bagenal, 1992) during the 1986 transit. This magnetic field can, to first order, be represented by a simple off-set tilted dipole (OTD). The components for an OTD for Jupiter and Uranus (Connerney, 1993) are compared in Table 2. Units are R_U (distance) and gauss (magnetic field amplitude) using the Voyager PDS coordinates while the Jovian coordinate system is SIII (Riddle and Warwick, 1976; Seidelmann and Divine, 1977). Similarly, Connerney also provided a detailed "Schmidt-Normalized" coefficients representation (Connerney et al., 1987) called the "Q_3" model (Table 3).

Based on Connerney's magnetic field models, FORTRAN programs have been constructed for computing the magnetic components and for estimating B (the magnetic field amplitude), B_{eq} (the magnetic field at the magnetic equator), B_{crit} (the lowest altitude value of the magnetic field along an L-shell), and L (the so-called L-shell)—all components required for modeling the trapped radiation belts. Sample outputs are presented in Figs. 9 and 10 for the magnetic field magnitude and L-shell values on the surface of Uranus for each model. While the Connerney Q_3 model is much more accurate than the OTD model, the latter runs significantly faster and, as shown in Figs. 9 and 10, the differences are not that great. A compiled version of the FORTRAN code for generating the OTD magnetic field components for input to UMOD is available on request from the authors.

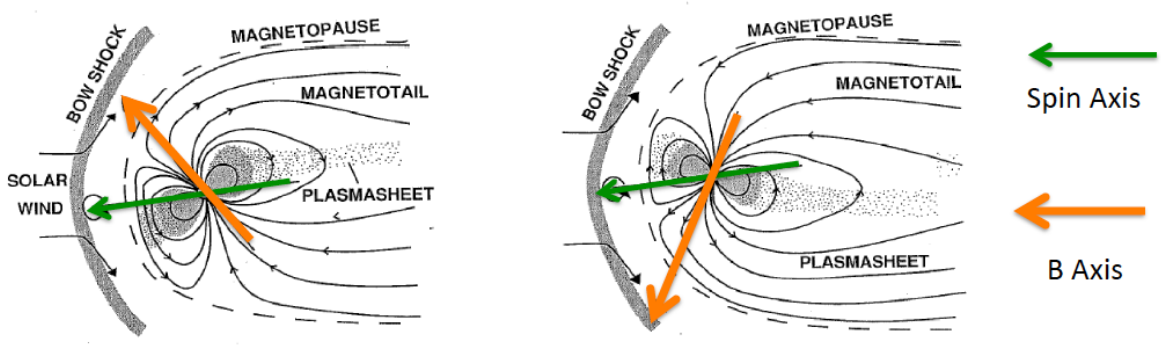

Figure 8. The magnetosphere of Uranus showing the ~60 deg tilt of the magnetic pole relative to the spin axis during the 1986 Voyager flyby. The two figures are half a planetary rotation apart (Bagenal, 1992). Modified with permission from the Annual Review of Earth and Planetary Sciences, Volume 20 © 1992 by Annual Reviews, http://www.annualreviews.org

Table 2. Comparison of the components of an OTD for Jupiter and Uranus (Connerney, 1993). Units are R_U (distance) and gauss (magnetic field amplitude) using the Voyager PDS coordinates while the Jovian coordinate system is SIII.

	Jupiter	Uranus
	Axis Offset	
Radial (R)	0.101	0.310
Rx	-0.092	-0.020
Ry	-0.042	0.020
Rz	0.009	-0.310
	Mag Vector	
Colat	10.770	60.000
WLONG	200.800	48.000
Magnitude	4.225	0.230
Rx	-0.738	0.133
Ry	0.280	-0.148
Rz	4.151	0.115

Table 3. Components of Connerney Q_3 model. Units are gauss.

Coefficient	Uranus Q_3
G01	0.11893
G11	0.11579
H01	-0.15684
G20	-0.0603
G21	-0.12587
G22	0.00196
H21	0.06116
H22	0.04759

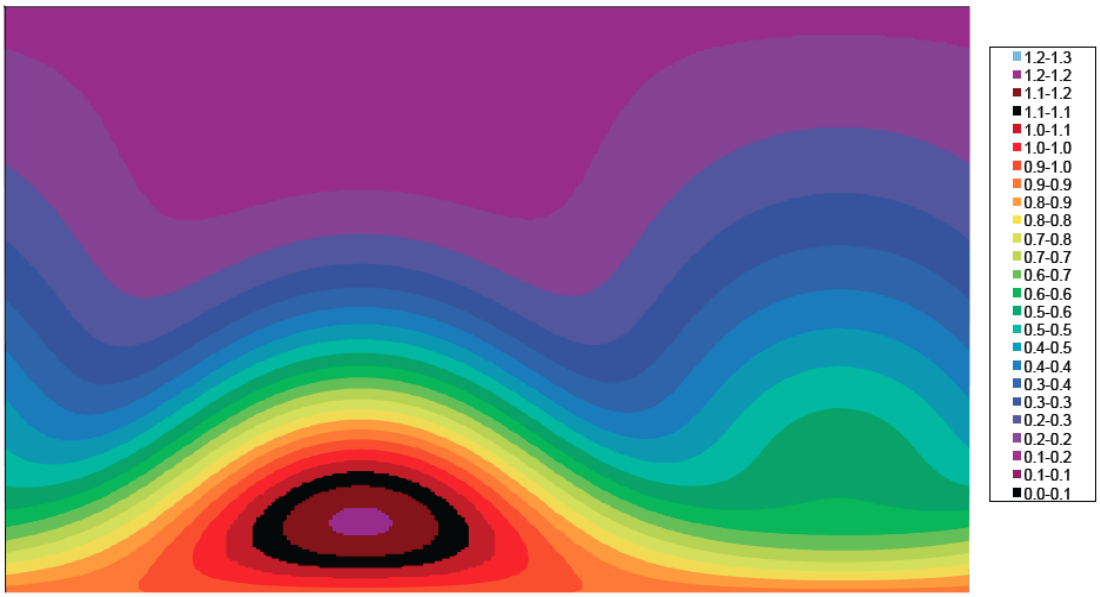

A) Magnetic Amplitude, gauss

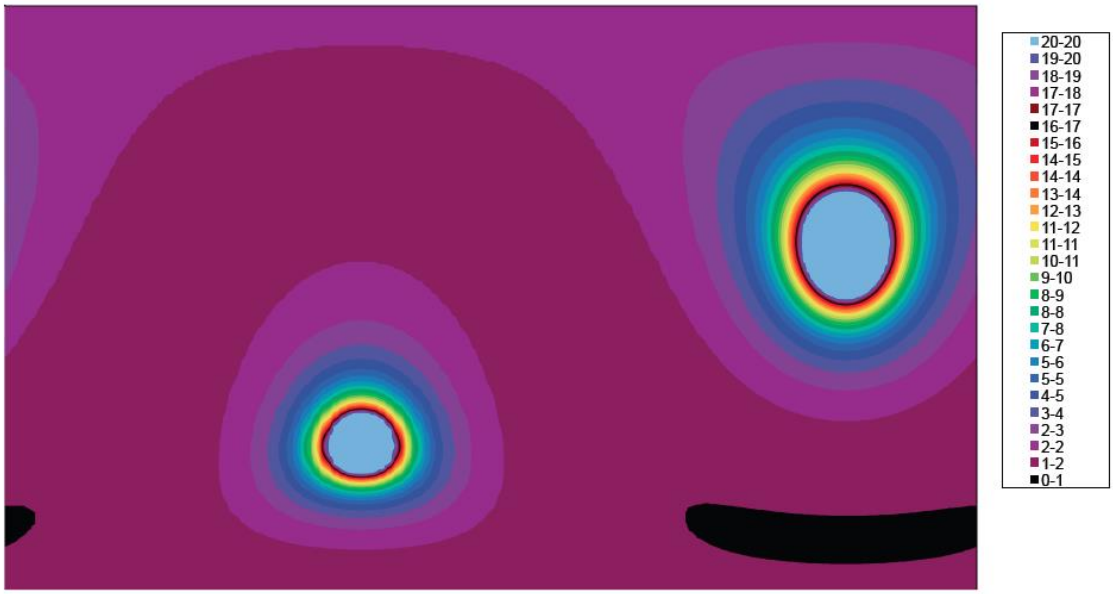

B) L-Shell values

Figure 9. Surface magnetic field parameters on Uranus for the Connerney OTD model: A) Magnetic field amplitude, B (in gauss); B) L-shell value. The two light blue regions in B mark the location of the magnetic poles.

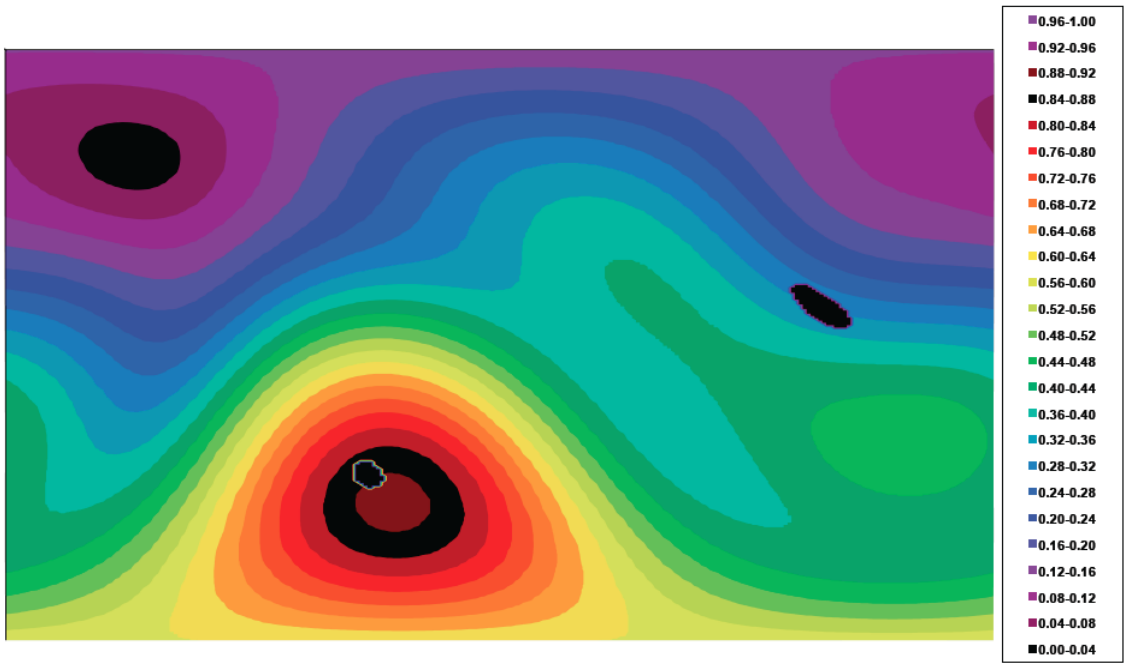

A) Magnetic Amplitude, gauss

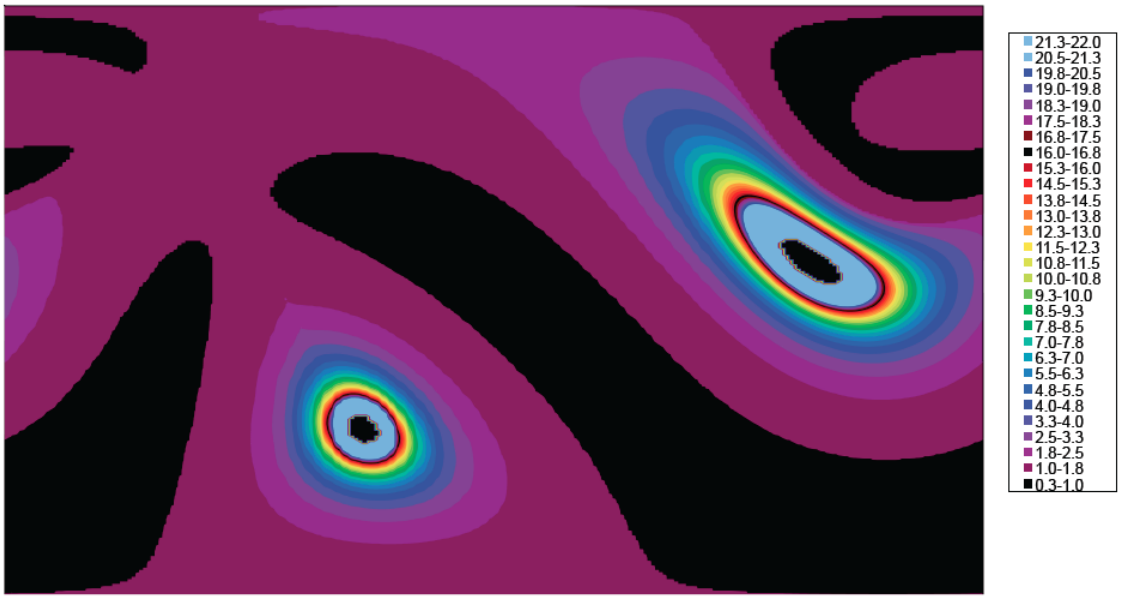

B) L-Shell values

Figure 10. Surface magnetic field parameters on Uranus for the Connerney Q_3 model: A) Magnetic field amplitude, B (in gauss); B) L-shell value. Note that the two black "spots" in A correspond to the magnetic poles shown in B and are indeterminate (L goes to infinity) in our field-line tracing program.

6. Selesnick and Stone Electron Radiation Model

The first component of the UMOD is based on the work of Selesnick and Stone (1991). They developed an energetic electron model at Uranus based on the Voyager 2 flyby data from two electron sensors on the electron telescope (TET) which was part of the Cosmic Ray Subsystem (CRS) experiment. The instrument provided estimates of the fluxes between ~0.7 MeV to ~2.5 MeV and for L-shell values between ~4.5 and 15 (based on the Q_3 magnetic field model). Their model provides the electron differential intensity as a function of energy and magnetic pitch angle assuming that the flux varies approximately with a power law in energy ($E^{-\gamma}$) and the pitch angle as $\sin^{2n}(\alpha)$. That is:

$$j(E,\alpha) = f(E)g(\alpha) = A_0 E^{-\gamma} \sin^{2n}(\alpha_0) \qquad (1)$$

where:

$j(E, \alpha)$	= electron differential intensity; $(cm^2\text{-sr-s-MeV})^{-1}$
$f(E)$	= electron differential intensity spectrum variation with energy; assumed to vary as $\sim A_0 E^{-\gamma}$ at the magnetic equator in Selesnick and Stone's model
$g(\alpha)$	= pitch angle variation of the Selesnick and Stone model; assumed to vary as $\sin^{2n}(\alpha)$
A_0, γ, n	= constants
E	= energy (MeV)
α_0	= pitch angle of particle relative to magnetic field direction at magnetic equator; related to α through Eq. 2 below
"0"	= subscript "0" refers to equatorial values

The local values at the spacecraft are related to the equatorial values by the following:

$$\sin^2\alpha = \frac{B}{B_0}\sin^2\alpha_0 \qquad (2)$$

$$A = \left(\frac{B_0}{B}\right)^n A_0 \qquad (3)$$

where:

α	= pitch angle of particle relative to magnetic field direction at spacecraft location
B	= magnitude of magnetic field at location
B_0	= magnitude of magnetic field at magnetic equator
A	= equivalent of A_0 in Eq. 1 at the spacecraft location

Selesnick and Stone (1991) estimated the above constants at the magnetic equator as functions of the magnetic L-shell based on fits to the Voyager data and the Q_3 magnetic field model. Their values are listed in Table 4. A FORTRAN program has been written that takes the values in

Table 4 and (given Equations 1, 2, and 3) computes the differential electron intensity versus pitch angle for a given B and L value. To compute the electron intensities for a trajectory or at a given spatial location around Uranus, B and L are calculated—using Eq. 1 these then give the electron pitch angle intensities at the B and L location(s). These values are integrated over pitch angle (0–180 deg) to give the omni-directional differential flux (units of $(cm^2\text{-s-MeV})^{-1}$). Figure 11 is a plot of the omni-directional electron integral fluxes for E>1 MeV for a meridional cut idealized dipole coordinates (R–γ) intended to replicate Plate 1 in Selesnick and Stone (1991).

Note: It was found that to get numeric agreement between their study, our study, and Mauk et al. (1987), it was necessary to assume that Selesnick and Stone (1991) did not multiply the contours by 4π to covert to omni-directional flux in performing the pitch angle integral—that is, we had to divide our omni-directional flux by 4π to get agreement. Their quoted units of electrons/cm^2-s (shown in Fig. 11) should probably be electrons/cm^2-sr-s.

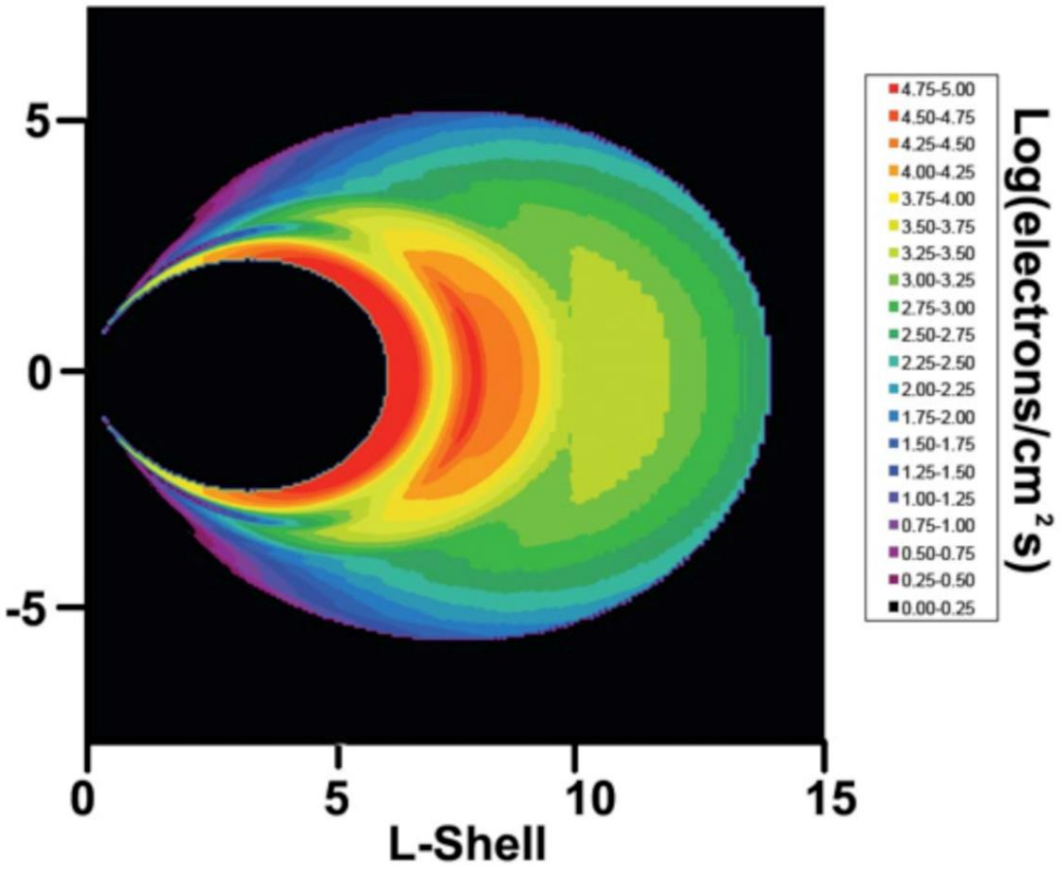

Figure 11. Contour plot in idealized dipole coordinates (R–λ) for electron integral fluxes for E>1 MeV.

Units are given to the right of the figure. To bring about agreement with Plate 1 in Selesnick and Stone (1991), our omni-directional values have been divided by 4π (we believe the units should actually be (electrons/cm^2-s-sr) in the figure and in their paper).

Table 4. Coefficients for the Selesnick and Stone (1991) model of the Uranian electron environment.

The values (at the magnetic equator) are used in Eq. 1 to compute the electron differential intensity versus pitch angle and energy.

L	N	γ	A_0
6.57	1.415	5.216	1.77E+05
6.87	1.253	5.184	1.12E+05
7.07	0.931	5.221	5.12E+04
7.29	0.35	4.361	8.21E+03
7.48	0	5.643	2.93E+03
7.63	0.143	4.514	1.40E+03
7.82	1.422	5.689	5.35E+03
7.92	1.955	6.534	9.74E+03
8.02	2.595	6.328	2.01E+04
8.1	3.093	7.429	3.72E+04
8.17	3.478	6.436	5.16E+04
8.26	3.122	6.588	4.40E+04
8.36	4.221	6.247	1.20E+05
8.7	1.778	6.149	1.90E+04
8.83	1.734	6.145	1.83E+04
8.98	1.757	6.269	1.83E+04
9.14	1.872	5.894	1.68E+04
9.31	1.782	5.932	1.45E+04
9.49	1.777	5.862	1.12E+04
9.68	1.818	5.718	8.48E+03
9.9	1.65	5.912	4.92E+03
10.13	1.9	5.789	3.40E+03
10.38	1.709	6.058	1.90E+03
10.65	1.411	6.532	1.44E+03
10.92	1.481	6.088	1.48E+03
11.24	1.839	7.317	2.43E+03
11.58	1.869	6.135	2.33E+03
11.94	1.877	6.684	2.29E+03
12.31	1.851	7.146	2.01E+03
12.72	1.785	6.673	1.52E+03
13.14	1.652	6.942	1.06E+03
13.61	1.446	6.651	6.57E+02
14.13	1.579	6.545	4.89E+02
14.72	1.328	7.111	2.53E+02

7. Low-Energy Charged Particle Data Description

The second primary source of particle data from the Voyager flyby is from the "Low-Energy Charged Particle" (LECP) investigation on Voyager 2. This instrument measured electrons with energies from 22 keV to greater than 1.2 MeV and protons (actually Z≥1) from 29 keV to 3.5 MeV). By sector (e.g., pitch angle) and sector averaged observations were provided to the PDS in the form of differential fluxes in units of (n#/cm^2-s-sr-keV). Here the latter data (sector averaged fluxes) averaged over 4-minute data intervals near closest approach (Day 24, Hours 13 to 22, 1986) for the channels given in Table 5 (adapted from Mauk et al., (1987) Table 1) form the basis of the UMOD analysis.

Table 5. Characteristics of the Voyager 2 LECP channels used in this study.

"Geo Mean Energy" is the geometric mean energy (sqrt(E_{lo}*E_{hi})) assumed for the channel. The e- 0.183-0.5 MeV channel was included in the study but not in the fitting process as the data were very sporadic compared to the other channels. Channel characteristics are from Mauk et al. (1987), Table 1.

Energies (MeV)	Geo Mean Energy (MeV)	dE (MeV)	εGEO Factor*
e- 0.022-0.035	0.028	0.013	0.006
e- 0.035-0.061	0.046	0.026	0.006
e- 0.061-0.112	0.083	0.051	0.006
e- 0.112-0.183	0.143	0.071	0.0039
e- 0.183-0.5	0.302	0.317	0.002
e- 0.252-0.48	0.348	0.228	0.0081
e- 0.480-0.853	0.640	0.373	0.0035
e- 0.853-1.2	1.012	0.347	0.00017

Energies (MeV)	Geo Mean Energy (MeV)	dE (MeV)	εGEO Factor
H^+ 0.028-0.043	0.035	0.015	0.113
H^+ 0.043-0.080	0.059	0.037	0.113
H^+ 0.08-0.137	0.105	0.057	0.113
H^+ 0.137-0.215	0.172	0.078	0.113
H^+ 0.215-0.54	0.341	0.325	0.113
H^+ 0.54-0.99	0.731	0.45	0.113
H^+ 0.99-2.14	1.456	1.15	0.113
H^+ 2.14-3.5	2.737	1.36	0.113

*Efficiency × geometric factor (units cm^2-sr)

In addition to the PDS, the Mauk et al. (1987) study provided graphs of the raw electron and proton count rate data for the period near closest approach to Uranus. This allowed a check on the quality of the PDS data. Their Figs. 8 and 9 show plots of the raw count rate data that were scanned, digitized, and compared with the PDS data using the conversion factors in Table 5—two sample plots overlaying the PDS, Mauk et al. (1987) count rate data, and Uranus radiation model predictions are provided in Figs. 12 and 13 of this document. The computed flux values from the scans agreed within a few per cent of the PDS data validating the use of that data set for our modeling efforts. Expanding on this analysis, the PDS data at various energies for the electrons and protons are compared in later sections to the UMOD model predictions versus time, L-shell, and each other and are discussed in detail in that section.

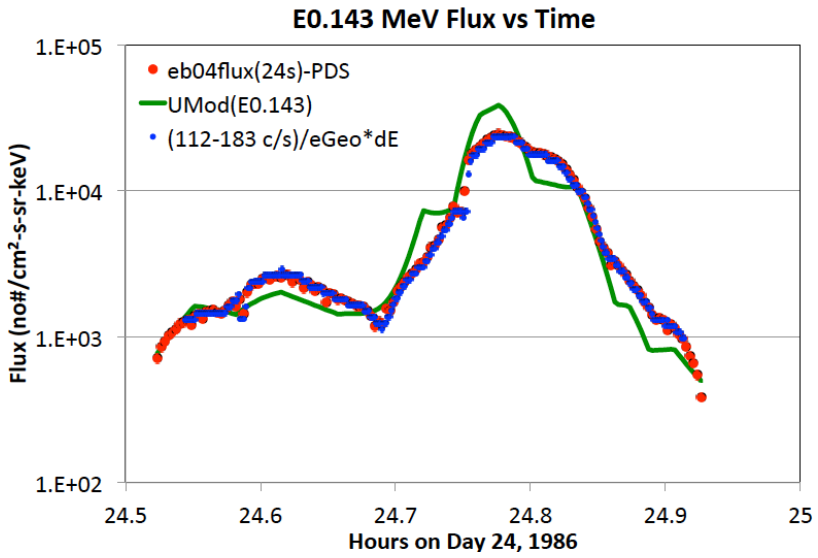

Figure 12. PDS electron flux data (red) versus SCET during the encounter for the 112–183 keV channel compared with scanned count rate data (blue) from Mauk et al. (1987), Fig. 8, converted to fluxes (Table 5). UMOD model fluxes are shown in green.

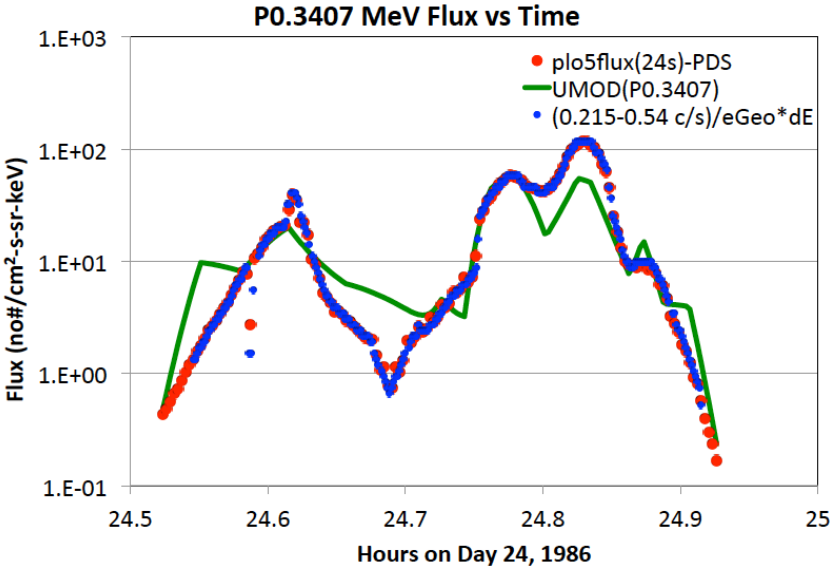

Figure 13. PDS proton flux data (red) versus SCET during encounter for the 215-540 keV channel compared with scanned count rate data (blue) from Mauk et al. (1987), Fig. 9, converted to fluxes (Table 5). The UMOD model fluxes are shown in green.

Given the LECP particle data, the Q_3 and OTD magnetic field components were then computed for the flyby observations sequence for each 4 minute average interval. Figures 14 and 15 compare the PDS flux data with the UMOD model predictions for L-shell variations. Note that there are large differences between the in and out trajectories versus L-shell between ~6–8 and 11–12 for the protons. The reason for this is that the data were often taken at very different magnetic latitudes for each L-shell. As will be discussed in the next section, comparing these differences will allow a determination of the pitch angle distributions along the L-shell. The

PDS data are of particular importance because they will be used to validate the UMOD radiation model by comparing the predictions of the model to the actual fluxes.

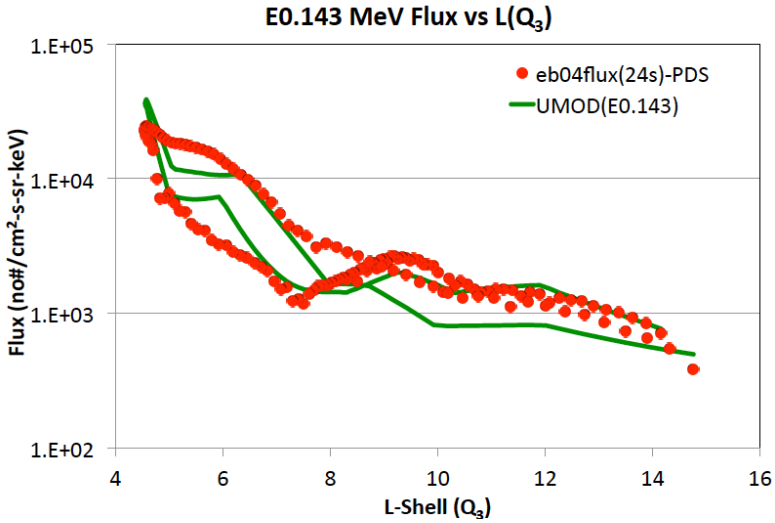

Figure 14. Electron flux data versus L-shell (Q_3) from the PDS (red) for the 112-183 keV channel compared with the Uranian model fluxes (green).

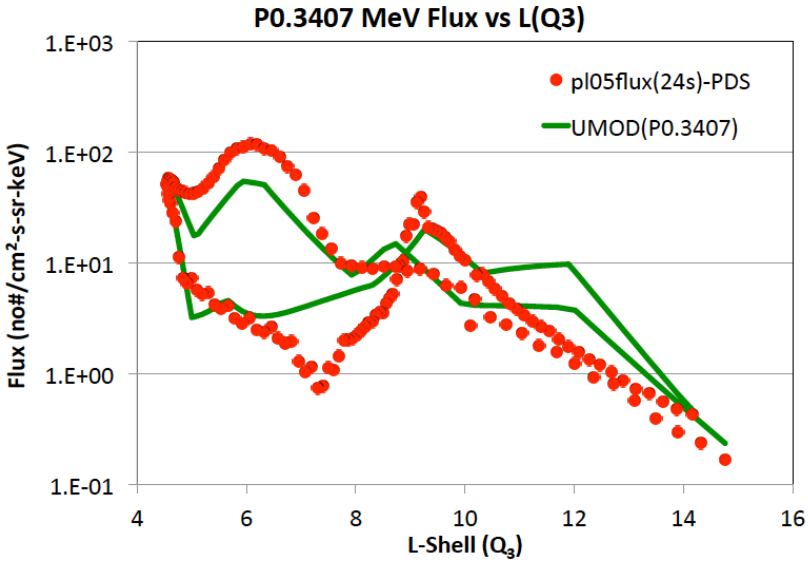

Figure 15. Proton flux data (red) versus L-shell (Q_3) from the PDS for the 215-540 keV channel compared with the Uranian model fluxes (green).

8. Analysis of the Differential Flux Intensity Spectra

As the first step in developing a model capable of predicting the Uranian electron and proton fluxes, published particle spectra were fit in terms of energy and L-shell/SCET. These spectra form the core of the UMOD model to be presented here. Selesnick and Stone (1991), for example, published a differential electron spectrum at ~13:14 SCET on 24 January 1986 incorporating both the TET and LECP data between 100 keV and 5 MeV. This spectrum is presented in Fig. 16 (e.g., purple symbols for the TET, red for the LECP). Similarly, Mauk et al. (1987) have provided LECP electron and proton differential spectra at 8 other locations (their Figure 10). A sample of one of their proton spectra is plotted here as Fig. 17 and shows their estimates of the proton differential intensities averaged over all the sectors (e.g., pitch angles) at one of the 8 selected locations (SCET 13:58). Table 6 provides the SCET times, L-shells for the Q_3 magnetic field model, and radial distances for the Selesnick and Stone and Mauk et al. spectra. All the electron and proton spectra used in this study and our fits are plotted in Appendix A1.

The pairs of differential spectra were fit using a standard regression technique in Excel to equations of the form:

$$Log_{10}(f'(E)) = A_0 + A_1 Log_{10}\big(f(E)\big)^1 + A_2 Log_{10}\big(f(E)\big)^2 + A_3 Log_{10}(f(E))^3 + A_4 Log_{10}(f(E))^4 \quad (4)$$

Where:

- E = Energy (keV)
- F = Differential intensity spectrum at energy E and given location (units are $(cm^2\text{-s-sr-keV})^{-1}$)
- f' = Predicted differential intensity spectrum at energy E and SCET t (units are $(cm^2\text{-s-sr-keV})^{-1}$)
- A_i = Regression fit constants where i = 0, 1, 2, 3, for 4 [corresponding to (E0, E1, E2, E3, E4) for electrons and (P0, P1, P2, P3, P4) for protons in Table 7]

The constants and the regression coefficient, R^2, for each fit are listed in Table 7. Typical fits to the spectra are presented in Fig. 16 and 17 (the orange curves). The complete set of spectra from Mauk et al. (1987) and of the fits to the differential electron and proton spectra are provided in Appendix A1.

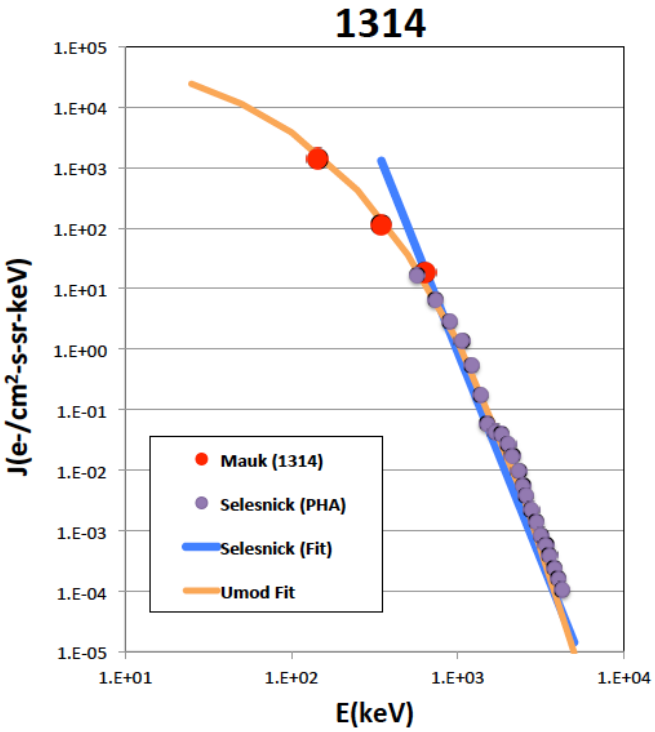

Figure 16. In-situ electron flux measurements compared with UMOD fits at 13:14 SCET. The purple symbols are the differential intensities versus energy from the Voyager 2 TET pulse height analyzer (Fig. 3, Selesnick and Stone, 1991) at Uranus. The three red symbols correspond to LECP measurements at the same time. The orange curve is the smoothed fit from Table 7 to the points—the blue line is the power law fit from Selesnick and Stone (1991) for ~0.5-1 MeV. See Appendix A1 for more examples of the fits.

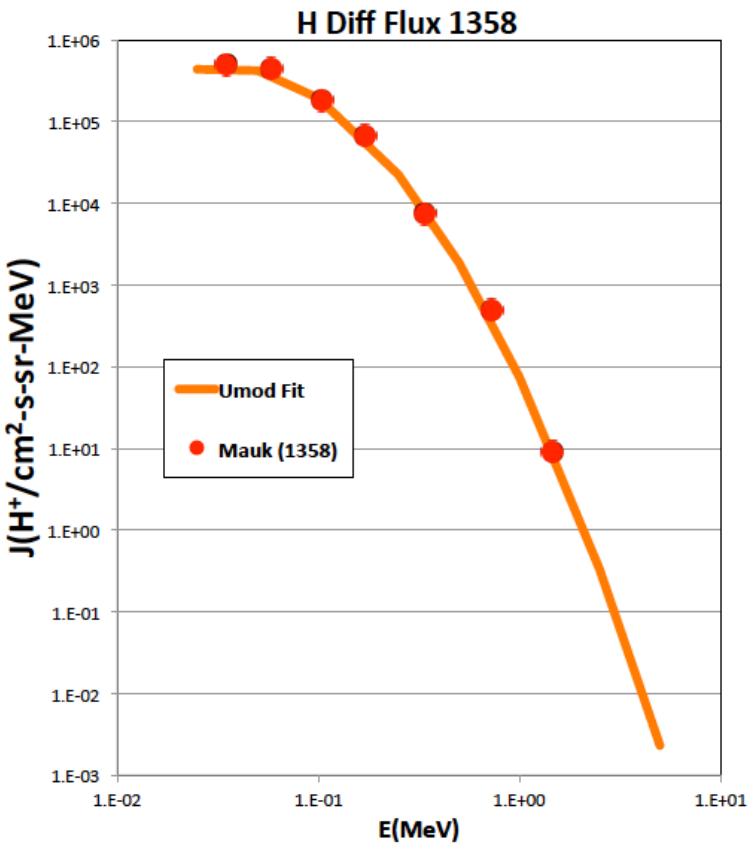

Figure 17. Comparison of a Table 7 fit to a LECP proton (SCET 1358) flux spectrum from Mauk et al. (1987), Fig. 10. See Appendix A1 for more examples of the fits.

Table 6. SCET, radial distance (R_u), latitude (degree), west longitude (degree), magnetic field amplitude (Q_3), and L-shell (Q_3) for the spectra used in this study.

SCET	R_u	Latitude	West Long	$B_{s/c}$(G)	L-Shell (Q_3)
10:58	16.3	57.9	114	7.81E-05	30.4
12:34	12.9	53.5	155	1.20E-04	14.9
13:13	11.5	51	171	1.51E-04	12.1
13:58	10	47.3	190	2.19E-04	10.1
14:45	8.44	41.7	211	3.89E-04	8.81
15:46	6.59	31.1	238	9.63E-04	8.09
17:49	4.21	-18.3	297	4.12E-03	5.12
18:37	4.46	-44.3	323	3.18E-03	4.59
20:02	6.32	-72.6	25.9	1.10E-03	6.44

Table 7. Regression fit constants and coefficients defined in Eq. 4 for the differential intensity spectra in Figs. 16 and 17 and Appendix A1. E0–E4 are the electron constants while P0–P4 are the proton constants. Units are $(cm^2\text{-s-sr-keV})^{-1}$. The proton spectra for SCET 1314 and 1358 are assumed to be the same.

R_U	SCET	$L(Q_3)$		E4	E3	E2	E1	E0	R^2
4.46	1838	4.59		0	-0.4755	2.3287	-4.4556	8.1066	0.99366
4.21	1749	5.12		0	-0.1512	-0.181	1.0809	4.0393	0.99872
6.32	2002	6.43		0	-0.7491	4.449	-10.231	13.008	0.99244
6.59	1546	8.09		0	-0.5259	1.9963	-3.3128	6.4132	0.99628
8.44	1446	8.82		0	-0.5075	2.4099	-5.1891	8.413	0.99841
10.04	1358	10.1		0	-0.2715	0.6309	-1.1933	5.5862	0.9978
11.53	1314	12.1		0	-0.4193	1.3549	-2.2664	6.0515	0.99651
12.91	1234	14.9		1.002	-10.288	36.299	-55.451	35.223	0.99866
16.26	1058	30.4		0	-0.8455	3.4088	-6.8146	8.0592	1

R_U	SCET	$L(Q_3)$		P4	P3	P2	P1	P0	R^2
4.46	1838	4.59		0	0	-0.8306	2.1057	1.7996	0.99892
4.21	1749	5.12		0	0	-1.2369	2.7867	1.8478	0.99099
6.32	2002	6.43		0	-1.3384	9.1178	-21.668	20.288	0.99699
6.59	1546	8.09		0	0	-1.0143	2.2215	1.5699	0.99414
8.44	1446	8.82		-1.6373	14.697	-49.661	73.061	-36.53	0.99968
10.04	1358	10.1		0	0	-1.7647	5.4052	-1.432	0.99865
11.53	1314	12.1		0	0	-1.7647	5.4052	-1.432	0.99865
12.91	1234	14.9		0	0	-1.8326	4.7498	-0.5394	0.99662
16.26	1058	30.4		0	0	0	-3.6406	6.6878	0.99118

9. Pitch Angle Distributions

As illustrated in Figs. 14 and 15, there can be large differences between Voyager 2 measurements at the same L-shell positions. The reason for this difference is believed to be in large part due to pitch angle variations. As discussed in both Mauk et al. (1987) and Selesnick and Stone (1991), to first order the pitch angle variations can be described in terms of Eq. 1 where the pitch angle variations are assumed to be proportional to $sin^{2n}(\alpha)$ where n is a "to be determined" fit parameter and α is the magnetic pitch angle of the particle relative to the magnetic field vector at the specified location. Both Mauk et al. (1987) and Selesnick and Stone (1991) have estimated the pitch angle power n along the Voyager trajectory. Selesnick and Stone's estimates of n are provided in Table 4. Mauk et al. (1987) provided snapshots (their Fig. 13) of the normalized pitch angle variations over 48 s along the Voyager trajectory at 10 locations. The snapshots were for the 43–80 keV and 540–990 keV protons and for the 22–35 keV and >480 keV electrons. A standard regression technique was used to fit the normalized plots in terms of $sin^{2n}(\alpha)$. Table 8 lists the fits and regression fit coefficients. The original LECP data and the regression fit predictions for $2n$ are plotted in Fig. 18. Figure 19 illustrates the final fits to the $2n$ values presented in Table 8. The two fit equations are as follows (note: the fits are both to the "lo" and "hi" values simultaneously):

$$2n_e = -0.0241\ L^3 + 0.6513\ L^2 - 5.5149\ L + 15.584 \quad (5)$$

$$2n_p = -0.0291\ L^3 + 0.829\ L^2 - 7.4794\ L + 22.693 \quad (6)$$

Table 8. Regression fits to $A_0\ sin^{2n}(\alpha)$ for Fig. 18. R^2 is the regression coefficient for each fit. As the pitch angle curves were normalized prior to fitting, A_0 should ideally be ~1 for all fits.

				H^+ 43-80 keV			e- 22-35 keV		
R_U	L	SCET	No#	2n	R^2	A_0	2n	R^2	A_0
12.1	13.082	1245-1309	1	2.574	0.947	0.988	1.368	0.969	1.012
11	11.25	1322-1334	2	2.611	0.952	1.018	1.427	0.961	1.022
9	9.1611	1422-1458	3	0.785	0.799	0.852	0.936	0.970	0.936
6.9	8.1785	1521-1546	4	0.819	0.984	0.937	0.507	0.987	0.970
5.5	7.8508	1625-1626	5	1.002	0.989	1.033	0.582	0.999	1.024
4.35	5.8719	1713-1738	6	0.908	0.820	0.950	0.670	0.989	1.009
4.2	5.0043	1801-1802	7	1.274	0.647	0.890	1.053	0.941	1.034
6	6.0423	1925-2013	8	7.393	0.990	0.998	2.945	0.777	0.992
7.95	8.8685	2038-2114	9	1.435	0.872	0.997	1.121	0.859	0.990
9.9	12.858	2150-2202	10	0.557	0.852	0.973	0.203	0.844	0.984
				H^+ 540-990 keV			e- >480 keV		
R_U	L	SCET	No#	2n	R^2	A_0	2n	R^2	A_0
12.1	13.082	1245-1309	1	2.312	0.505	0.966	4.331	0.872	0.942
11	11.25	1322-1334	2	0.046	0.235	0.975	1.882	0.972	0.990
9	9.1611	1422-1458	3	1.942	0.977	1.111	1.596	0.980	1.032
6.9	8.1785	1521-1546	4	0.589	0.853	0.948	0.875	0.859	0.903
5.5	7.8508	1625-1626	5	1.352	0.827	1.128	0.756	0.956	1.039
4.35	5.8719	1713-1738	6	2.150	0.976	0.911	1.060	0.989	0.981
4.2	5.0043	1801-1802	7	3.431	0.925	1.139	1.451	0.974	0.997
6	6.0423	1925-2013	8	5.937	0.719	0.964	5.518	0.897	0.986
7.95	8.8685	2038-2114	9	3.924	0.734	0.955	1.557	0.689	0.999
9.9	12.858	2150-2202	10	0.772	0.701	0.951	1.716	0.877	0.939

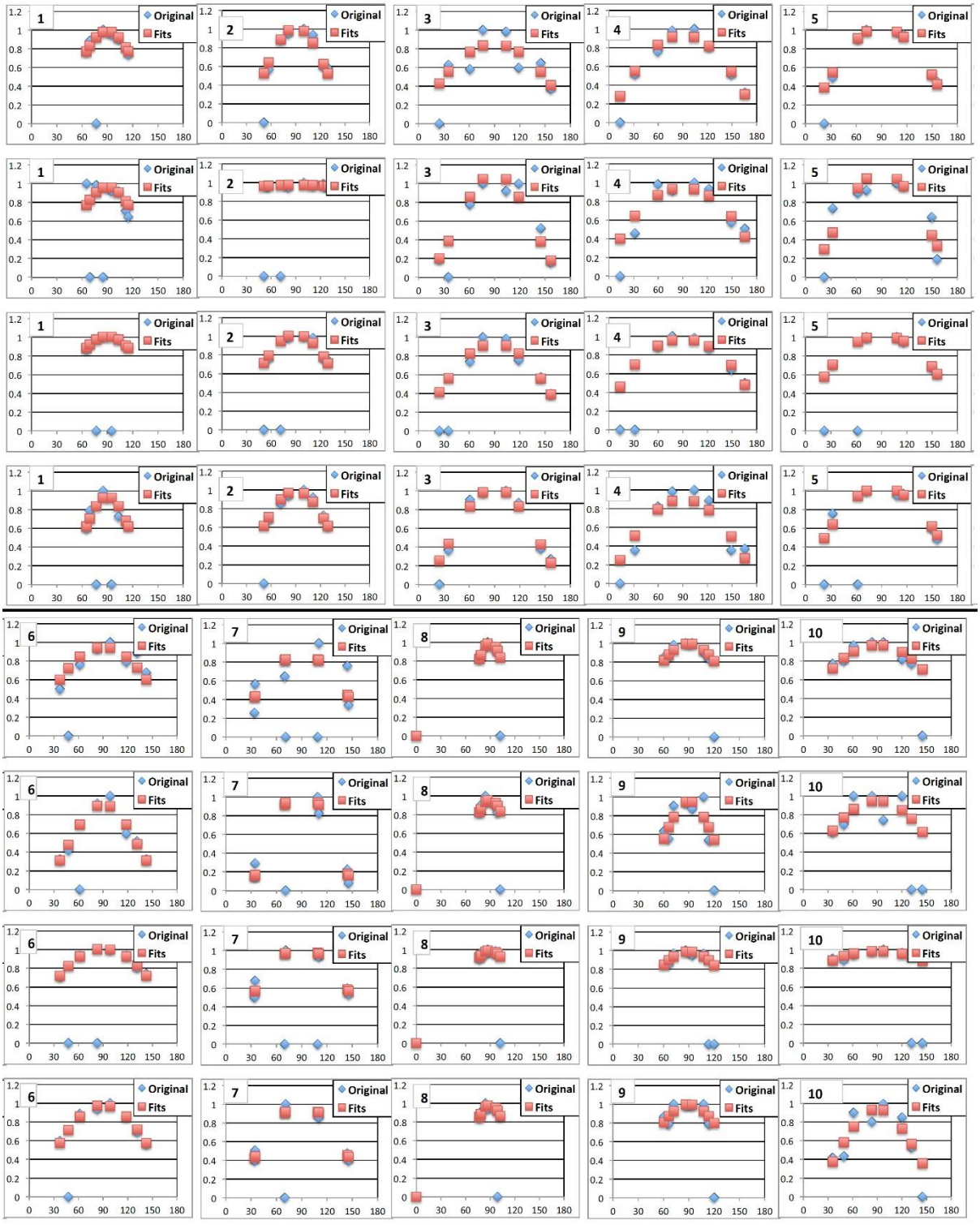

Figure 18. Fits to the pitch angle variations provided by Mauk et al. (1987) Fig. 13. The top two rows in each set correspond to the protons, the lower to electrons. The fit constants determined by linear regression are presented in Table 8.

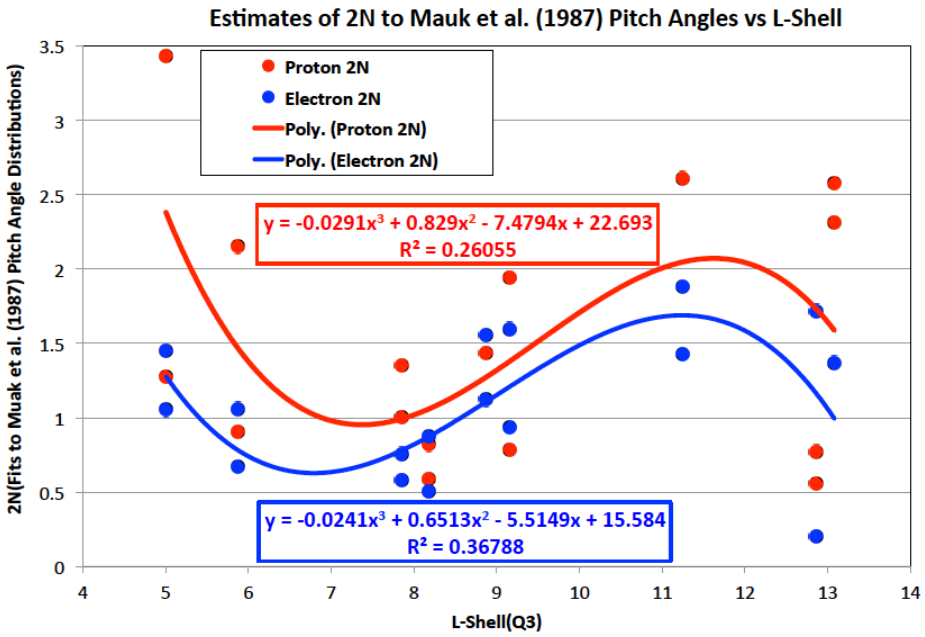

Figure 19. Fits to the "2*n*" values presented in Table 8 and based on the Mauk et al. (1987) pitch angle distributions of Fig.18. The fits are to both the "lo" and "hi" simultaneously.

The normalized pitch angle function multiplied by the sector averaged differential spectrum provides a complete definition of the particle distribution at the given location. To determine the differential "omni-directional" intensity at a point, one integrates that function over pitch angle. That is:

$$J(E) = \int_{-\pi}^{\pi} d\alpha \int_{0}^{2\pi} j(E,\alpha)\, sin(\alpha)\, d\phi = 4\pi \int_{0}^{\pi} [f'(E) sin^{2n}(\alpha)] sin\,(\alpha) d\alpha \qquad (7)$$

where:

$J(E)$ = omni-directional differential flux versus energy E; units are $(cm^2\text{-s-keV})^{-1}$

$j(E,\alpha)$ = angular differential flux versus energy E; assumed to be given by: $f'(E)\ \sin^{2n}(\alpha)$; units are $(cm^2\text{-s-sr-keV})^{-1}$

ϕ = angle normal to the magnetic field

α = pitch angle at location of spacecraft/observation

$f'(E)$ = measured particle differential intensity given by plots in Appendix A1 and Eq. 4 and averaged over the LECP sectors (Fig. 18, Table 8)

The units derived above are in $(cm^2\text{-s-keV})^{-1}$ for the "omni-directional fluxes". As the spectra in Fig. 17 are assumed to be averaged over the LECP sectors, dividing the omni-directional flux by 4π gives the proton and electron differential intensity spectra. That is:

$$I(E) = J(E)/4\pi \qquad (8)$$

where:

I(E) = sector averaged differential intensity spectra, units are now $(cm^2\text{-s-sr-keV})^{-1}$

Up to this point in the discussion the particle fluxes are computed at the location of the spacecraft/observation and, since the pitch angle distributions are normalized at that location, should simply reproduce the spectra in Appendix A1. To make the UMOD radiation model useful for all locations along a field line, however, the differential intensity spectrum f'_α needs to be transformed to the magnetic equator from the spacecraft location and the integration carried out over α_0 as opposed to α. To do this, Eqs. 2 and 3 need to be inverted to give the relevant variables in terms of the more general equatorial values:

$$\alpha_0 = sin^{-1}\left(\left(\frac{B_0}{B}\right)^{1/2}\sin(\alpha)\right) \tag{9}$$

$$f'_{\alpha_0}(E) = f'_\alpha(E)\left(\frac{B}{B_0}\right)^n \tag{10}$$

where:

f'_{α_0} = differential intensity at the equator
f'_α = differential intensity at the spacecraft

The "*n*" values (Eqs. 5 and 6) along with B at the spacecraft and B_0 (*B* at the equator) for the L-shell are then used to compute the "correction" factor, $(B/B_0)^n$, to f'_α to give f'_{α_0} at the magnetic equator. Various estimates of this factor versus L are plotted in Fig. 20. "A0p-Lo", "A0p-Hi", "A0e-Lo", and "A0e-Hi" are the values computed at each of the positions in Table 8. "A0p(Fig 10)" and "A0e(Fig 10)" correspond to the positions in Mauk et al. (1987) Fig. 10 and the "n" values given by Eqs. 5 and 6. The wide range of values indicates the difficulty in defining the equatorial corrections factor. "A0p(UMOD)" and "A0e(UMOD)" are the assumed UMOD values, initially based on the Fig. 10 values but subsequently adjusted to give a best fit to the actual data—their validity to be tested by comparison with the PDS database.

To summarize, the differential intensity and pitch angle distributions at the spacecraft location are transformed to the magnetic equator at the L-shell position for that observation. For an arbitrary location along the field line, the equatorial spectrum is then integrated over pitch angle. The limits on that integration are defined to be between the 90 deg pitch angle at the desired location (given by substituting 90 deg into Eq. 7) and the critical pitch angle for atmospheric absorption—the pitch angle at which a particle will be lost to the atmosphere. This angle, α_c, at the equator is computed by substituting α = 90 deg and $B = B_c$ in Eq. 9 where B_c is the value of the magnetic field at the top of the atmosphere on the field line. B_c is given by the following fit to the surface magnetic field at Uranus:

$$B_c = -1.7167624e\text{-}12\,L^6 + 6.9089932e\text{-}10\,L^5 - 1.1048113e\text{-}07\,L^4 + 8.9776988e\text{-}06\,L^3 - 3.9562106E\text{-}04\,L^2 + 9.5627844e\text{-}03\,L + 0.16708556 \tag{11}$$

where:

B_c = the minimum magnetic field strength at the top of the atmosphere

for specified magnetic L-shell passing through the desired location

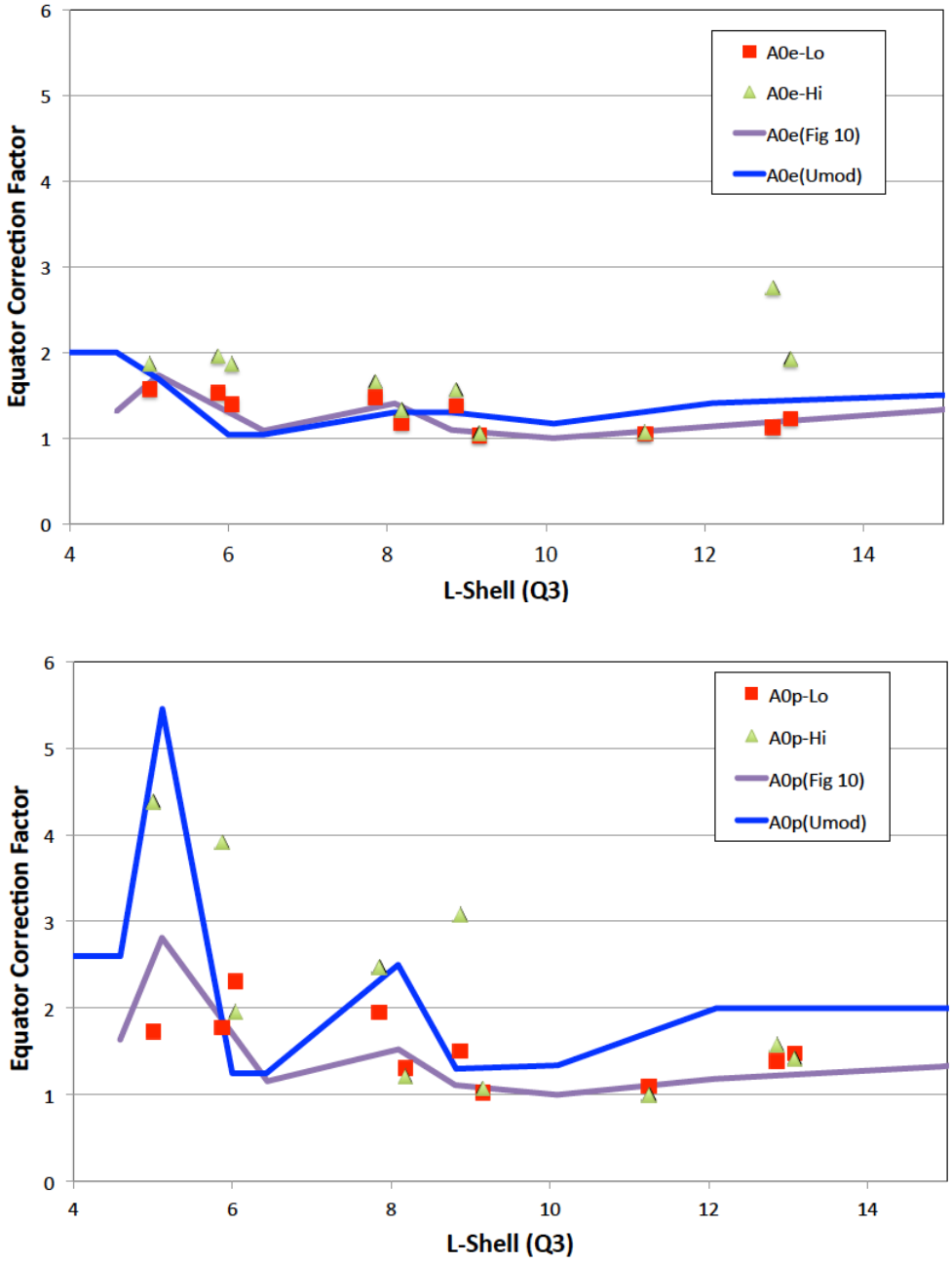

Figure 20. Various estimates of the correction factor $(B/B_0)^n$ at the magnetic equator as defined by Eq. 10, "*n*" from Fig. 19, and adjusted to give "best fits" to the PDS data for electrons (top) and protons (bottom). See text for an explanation of each estimate. The upper figure is for electrons, the bottom for protons.

10. UMOD Radiation Model

The preceding section has defined the primary elements of the UMOD Uranian radiation model. The steps, in order, to carry out the computation of the omni-directional differential intensity are as follows:

1. Define the L-shell, B(location), and B_{eq} as defined by the Q_3 magnetic field model of Connerney et al. (1987) for two L-shells for which spectra exist and bracket the L-shell passing through the desired location.
2. Compute the spectra versus energy for the protons and electrons as defined by Mauk et al. (1987) and Selesnick and Stone (1991) at the magnetic equator (that is, apply the equatorial correction factor to the original fitted spectra) for the two bracketing L-shell values.
3. Similarly, define the normalized pitch angle variations for the electrons and protons at the magnetic equator for both L-shells.
4. Integrate the resulting spectra at the two locations over pitch angle between the specified mirror point angle and Bc at the equator.
5. Linearly interpolate the Log10 of the intensity between the two bracketing estimates to give the value at the location and at the selected energy.
6. If the integral flux is desired, repeat at higher energies and numerically integrate to approximate the integral.

A compiled version of the UMOD program that accomplishes these steps is available on request. The model results are compared with the PDS data in Figs. 21–24 as functions of SCET and L-shell for the Voyager 2 flyby on January 24, 1986. The figures show that the UMOD model provides an adequate fit to the electron data over most of the time range. In L-shell, the electron data at the lowest energies appear to fall between the observed values in the range from ~6 to ~8 L. While over most of the energy range the proton data also appear to fit the PDS data, the lowest channel deviates from the PDS data by a large factor near closest approach-this behavior can also be see in the proton spectra fits in Fig. A1-1 where the polynomial fits appear to deviate from the Mauk et al. data in the lowest energy channel. The L-shell plots for the protons, similar to the electron plots, agree well except between ~6 to ~8 L. Here, however, the disagreement is primarily at the lowest energy channel and the three highest energy channels with the latter being over estimated during entry when the spacecraft was well above the magnetic equator. Clearly, further adjustments in the model are required between 6–8 L in the equatorial correction factor and probably in the pitch angle variations to account for these differences.

Figures 25 and 26 complete the comparisons between the PDS and UMOD by carrying out a cross-correlation analysis between the Log10 of the fluxes (or count rates) of the two data sets. The correlation values (and fit formulas) are tabulated in Tables 9 and 10.

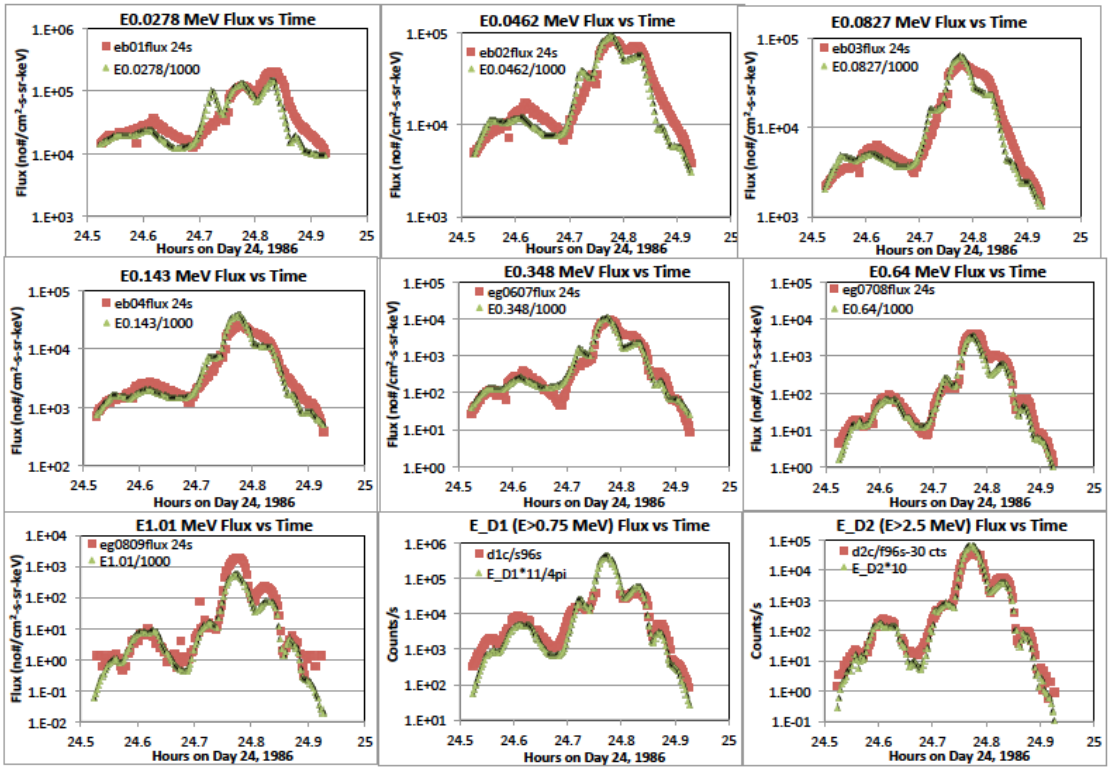

Figure 21. Electron flux data versus encounter time from the PDS for the specified energies compared with the corresponding UMOD model fluxes. Note that the last two channels are scaled to fit the PDS TET count rates which have not been converted to fluxes.

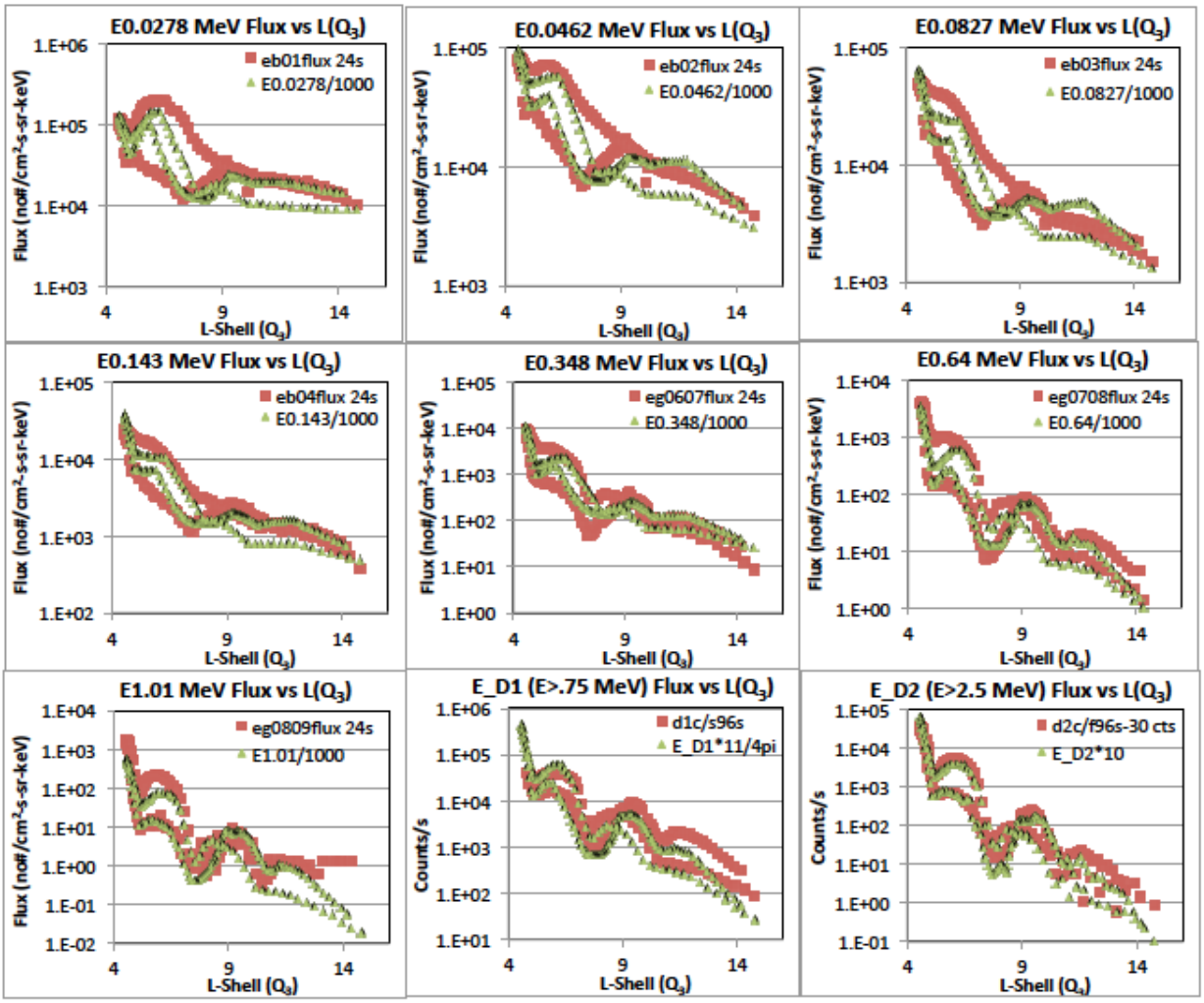

Figure 22. Electron flux data versus L-shell (Q_3) from the PDS for the specified energies compared with the UMOD model fluxes. Note that the last two channels are scaled to fit the PDS TET count rates which have not been converted to fluxes.

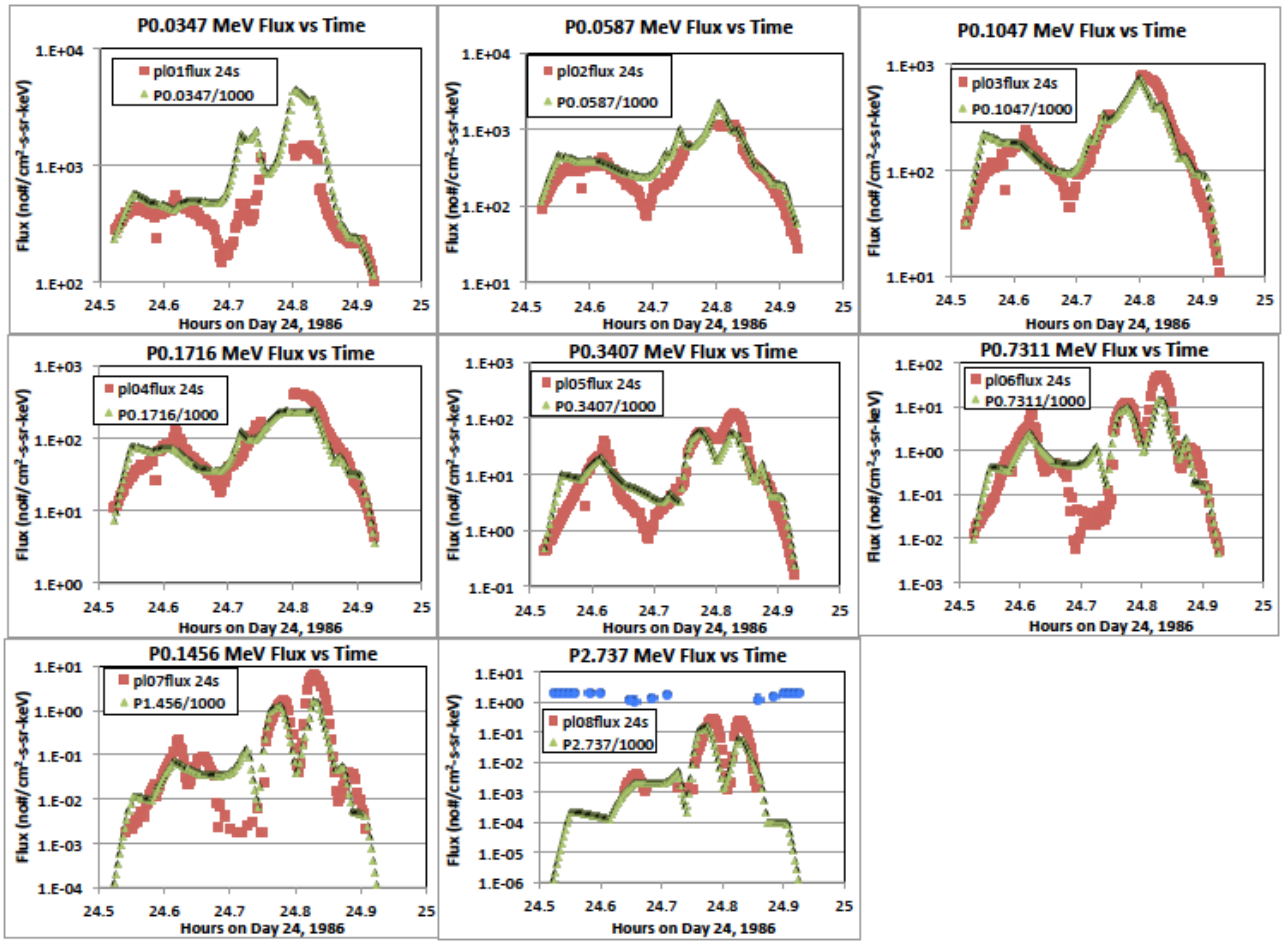

Figure 23. Proton flux data versus time from the PDS for the specified energies compared with the UMOD model fluxes.

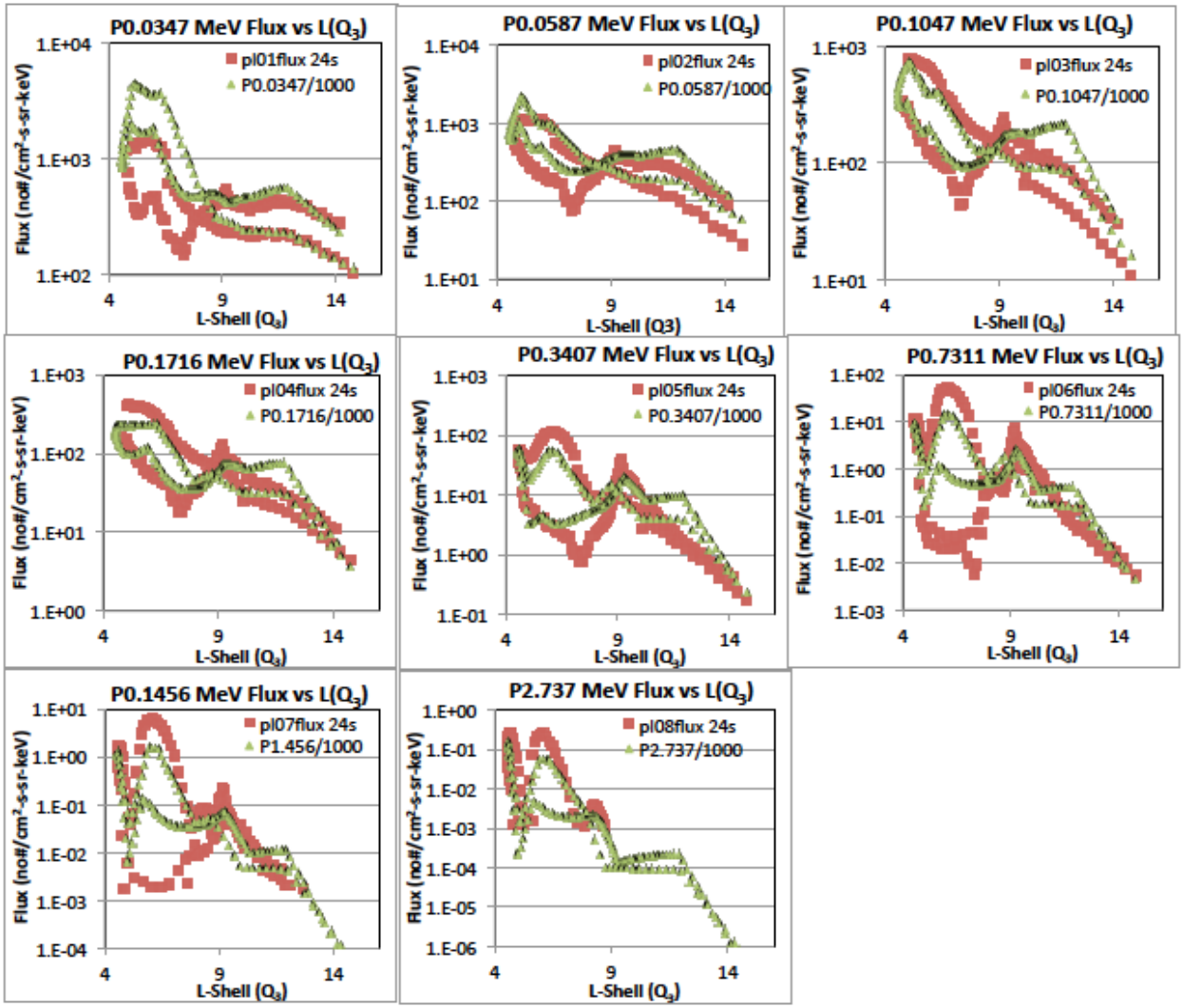

Figure 24. Proton flux data versus L-shell (Q_3) from the PDS for the specified energies compared with the UMOD model fluxes.

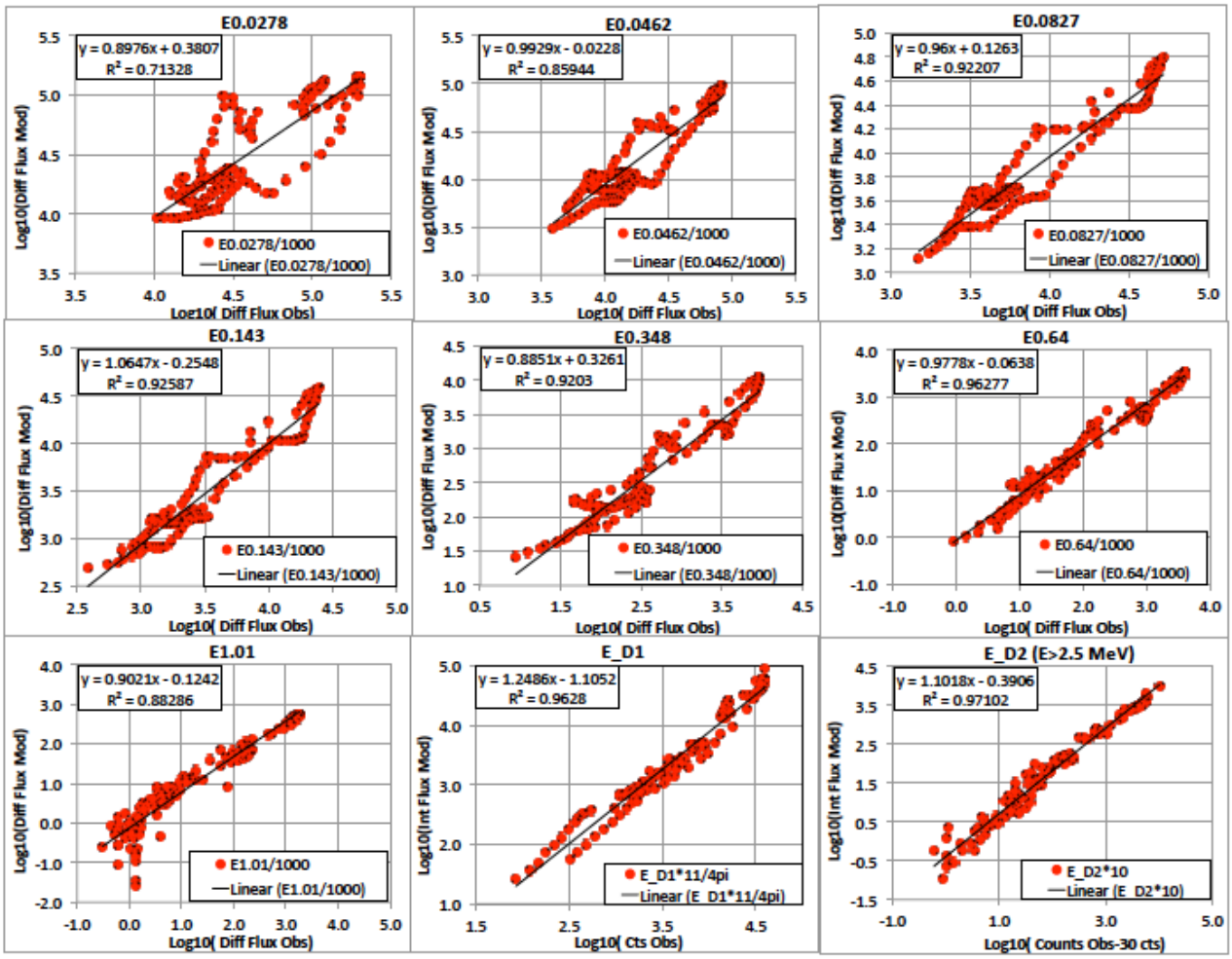

Figure 25. Linear correlations for the electrons between the PDS data and the UMOD model predictions. The regressions are carried out for the Log10 of the fluxes (or count rates) in all cases.

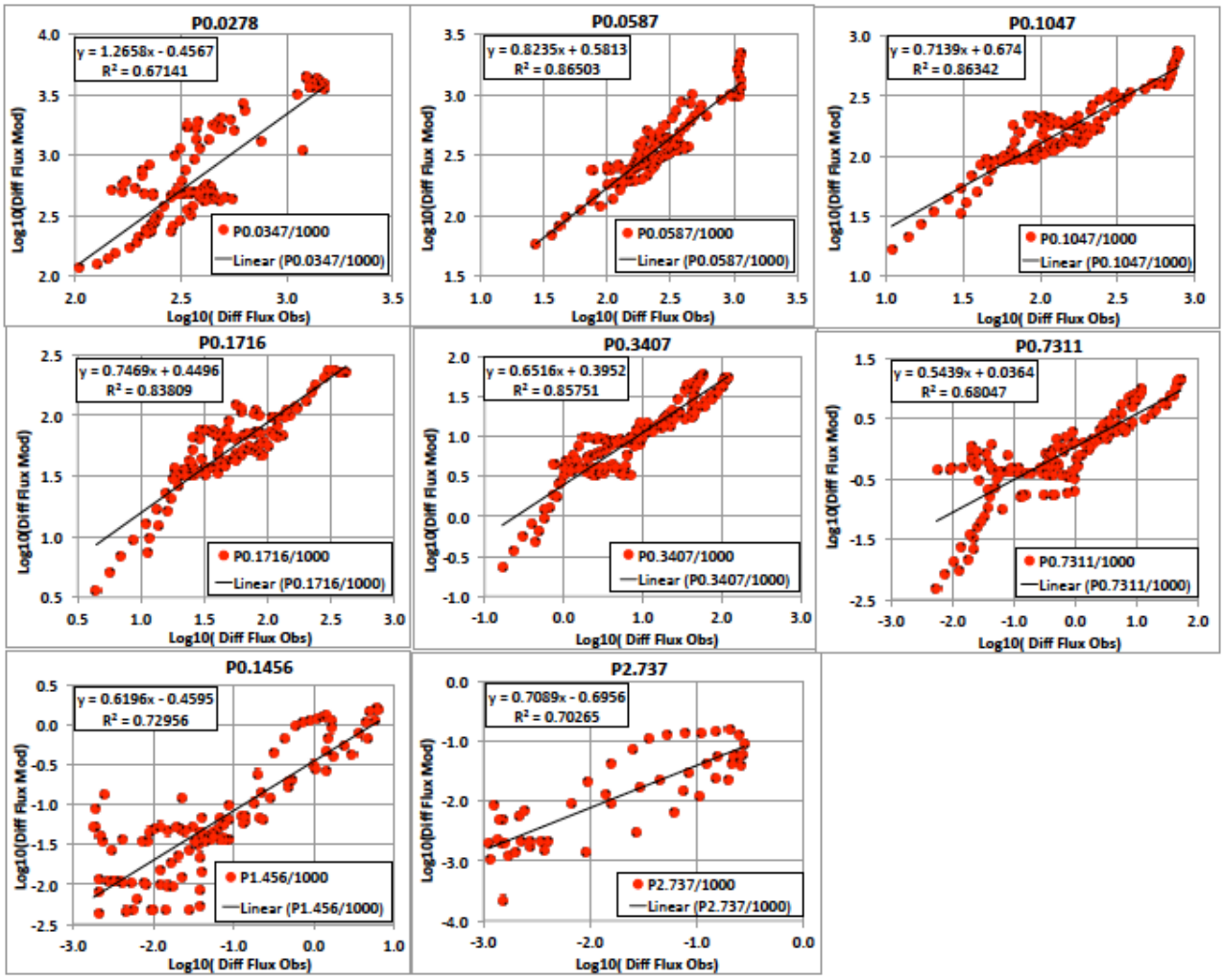

Figure 26. Linear correlations for the protons between the PDS data and the UMOD model predictions. The regressions are carried out for the Log10 of the fluxes (or count rates) in all cases.

The correlation results confirm the previous observations about the time and L-shell comparisons. In particular, the electron data show very high correlations coefficients except for the lowest 0.022–0.035 MeV channel. The predictions appear to be within a factor of 2 or better of the PDS data. The protons are not as well correlated as expected with correlation functions below 0.8 for the lowest energy channel (0.028–0.043 MeV) and for channels with energy above 0.54 MeV. The variations appear to be much higher also, approaching ~5. Again, as noted earlier, more effort in the future needs to be addressed towards improving the proton fits.

Table 9. Cross-correlations between the LECP PDS proton data and the UMOD predictions for the indicated energy intervals. Listed are the correlation coefficients, R^2, and the linear fits to the Log10 flux values (x = log10 (PDS), y = log10 (UMOD)).

Protons

Energy Interval (MeV)	Geometric Mean (MeV)	Correlation Coefficient (R^2)	Fit to Log10 Values
0.028-0.043	0.035	0.67141	y = 1.2658x - 0.4567
0.043-0.080	0.059	0.86503	y = 0.8235x + 0.5813
0.08-0.137	0.105	0.86342	y = 0.7139x + 0.674
0.137-0.215	0.172	0.83809	y = 0.7469x + 0.4496
0.215-0.54	0.341	0.85751	y = 0.6516x + 0.3952
0.54-0.99	0.731	0.68047	y = 0.5439x + 0.0364
0.99-2.14	1.456	0.72956	y = 0.6196x - 0.4595
2.14-3.5	2.737	0.70265	y = 0.7089x - 0.6956

Table 10. Cross-correlations between the LECP and TET PDS electron data and the UMOD predictions for the indicated energy intervals. Listed are the correlation coefficients, R^2, and the linear fits to the Log10 flux values (x = log10 (PDS), y = log10 (UMOD)). The E > 0.75 MeV and E > 2.5 MeV are for the TET counts per second data versus the UMOD flux predictions.

Electrons

Energy Interval (MeV)	Geometric Mean (MeV)	Correlation Coefficient (R^2)	Fit to Log10 Values
0.022-0.035	0.028	0.71328	y = 0.8976x + 0.3807
0.035-0.061	0.046	0.85944	y = 0.9929x - 0.0228
0.061-0.112	0.083	0.92207	y = 0.96x + 0.1263
0.112-0.183	0.143	0.92207	y = 0.96x + 0.1263
0.183-0.5	0.302	0.92587	y = 1.0647x - 0.2548
0.252-0.48	0.348	0.9203	y = 0.8851x + 0.3261
0.480-0.853	0.64	0.96277	y = 0.9778x - 0.0638
0.853-1.2	1.012	0.88286	y = 0.9021x - 0.1242
E>0.75	-	0.9628	y = 1.2486x - 1.1052
E>2.5	-	0.97102	y = 1.1018x - 0.3906

11. Applications of UMOD

Figure 27 illustrates a simple application of the UMOD model for mission planning-a plot of the 1 MeV electron integral flux and the 5 MeV proton integral flux contours for a meridian projection (idealized dipole coordinates R-λ). 1 MeV electrons and 5 MeV protons are roughly the cutoff energies for 50–100 mils of aluminum shielding, nominal shielding levels for a typical spacecraft design point. Clearly the region outside around 8 R_U should be very safe for total ionizing dose (TID) if that is a mission concern. Similarly, the UMOD can be used for the traditional purpose of modeling the TID for a spacecraft flyby. To be specific, Fig. 28 is a graph of the estimated TID for the Voyager 2 flyby. For a 100 mils of aluminum shielding, the total dose is on the order of only 100 rads (Si), an insignificant amount for the overall Voyager mission in comparison to its flyby of Jupiter. While orbital missions to Uranus will clearly see more significant TID levels, the UMOD indicates that radiation will likely not be a serious concern for mission designers if standard geosynchronous shielding or similar shielding design procedures are followed.

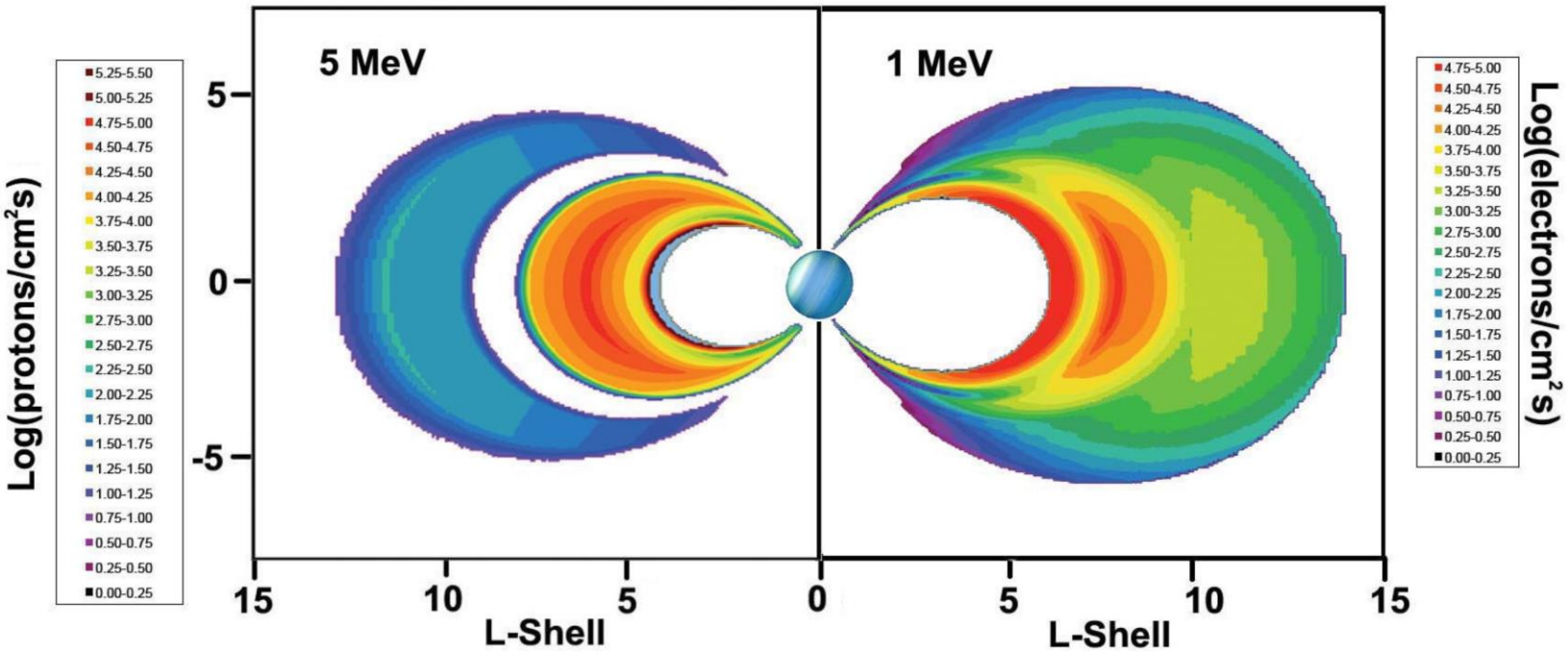

Figure 27. A plot of the 1-MeV electron and 5-MeV proton fluxes for a meridian profile (e.g., idealized dipole coordinates R-λ) of the Uranian radiation belts. Note that there is an absence of data inside ~4 R_U—this does not represent the absence of radiation flux in this region!

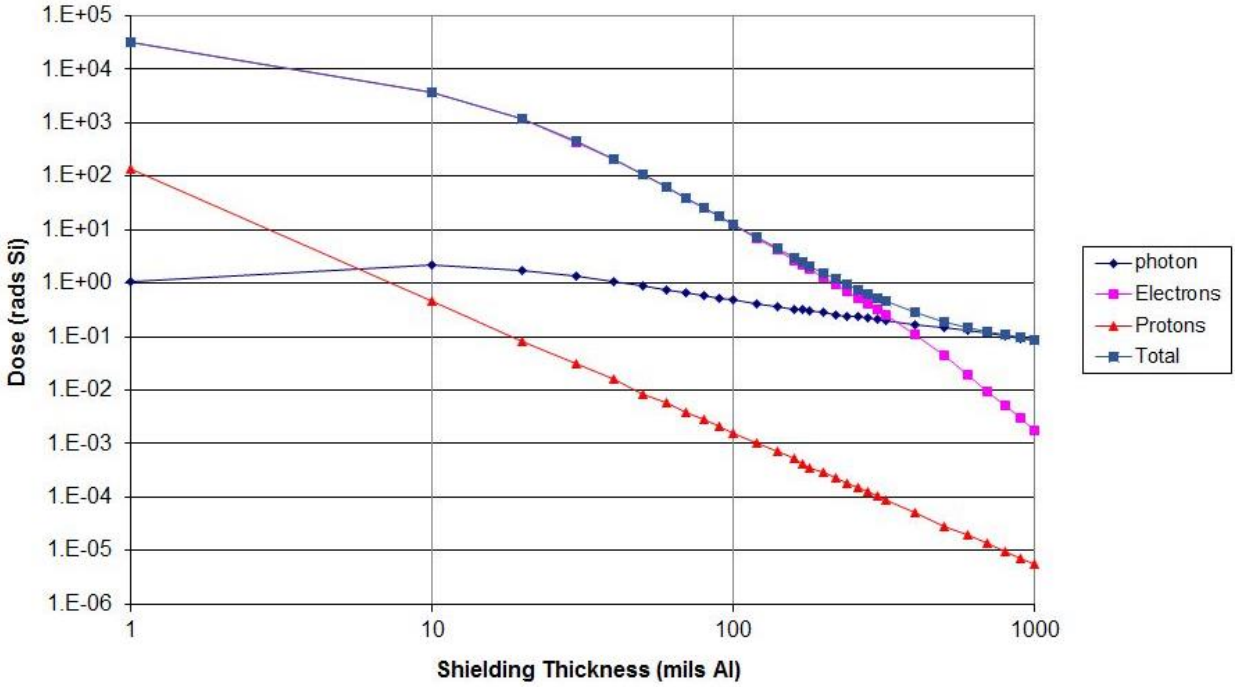

Figure 28. Graph of the estimated TID for the 1986 Voyager 2 flyby of Uranus using the UMOD radiation model.

12. Conclusion

The preceding has outlined the development of the UMOD Uranian radiation model. As a first step, an OTD magnetic field model was developed and compared with a more complex "Schmidt-Normalized" coefficient model called "Q_3" (Connerney, 1993; Connerney et al. 1987). These models were then used to compute B-L components for Uranus. Selesnick and Stone's (1991) first order electron radiation model for the energy range 0.7 to 2.5 MeV and between L values of 6 to 15 (based on Voyager TET data) was translated into a FORTRAN code that takes B-L coordinates and computes the omni-directional differential and integral electron fluxes. In the next phase, representative electron and proton data for the Voyager 2 flyby from the Voyager LECP instrument were analyzed and fit in energy and pitch angle. The resulting UMOD radiation model incorporates both sets of data and covers the range from ~0.022 MeV up to 2.5 MeV for the electrons and from ~0.028 MeV to 3.5 MeV for the protons. Data from the PDS were then used to test the electron and proton model predictions. The UMOD model was found to be within a factor of ~2 for the electrons and ~5 or better for the protons. The final product is in the form of a complete FORTRAN package capable of predicting the magnetic field and the electron and proton radiation environments along an arbitrary trajectory. Two useful applications of the model were presented and, though not included here, a movie was made of the Uranian radiation belts that illustrates their intricate and complex time variations over a Uranian rotation. The UMOD is now ready for mission design applications and for further testing and improvement.

13. References

Aoki, S.; Soma, M.; Kinoshita, H.; Inoue, K., "Conversion Matrix of Epoch B 1950.0 FK 4-Based Positions of Stars to Epoch J 2000.0 positions in accordance with the new IAU resolutions," *Astronomy and Astrophysics*, vol. 128, pp. 263–26, Dec. 1983

Bagenal, F., "Giant Planet Magnetospheres," *Ann. Rev. Earth Planet. Sci.*, vol. 20, pp. 289–328, 1992.

Connerney, J. E. P., "Magnetic Fields of the Outer Planets," *J. Geophys. Res.*, vol. 98, no. E10, pp. 18,659-18,679, October 25, 1993.

Connerney, J. E. P., Acuna, M. H., and Ness, N. F., "The Magnetic Field Of Uranus," *J. Geophys. Res.*, vol. 92, no. A13, pp. 15,329–15,336, December 30, 1987.

Desch, M. E., Connerney, J. E. P., and Kaiser, M. L., "The rotation period of Uranus," *Nature*, vol. 322, p. 42, July 3, 1986.

Evans, R., *PDS and Modern Uranus Co-ordinates*, IOM 5132-13-007 (also D-95199) (internal document), Jet Propulsion Laboratory, California Institute of Technology, Pasadena, CA, Jan. 21, 2013.

Mauk, B. H., Krimigis, S. M., Keath, E. P., Cheng, A. F., Armstrong, T. P., Lanzerotti, L. J., Gloeckler, G., and Hamilton, D. C., "The Hot Plasma and Radiation Environment of the Uranian Magnetosphere," *J. Geophys. Res.*, vol. 92, no. A13, pp. 15,283–15,308, December 30, 1987.

Ness, N. F., Acuna, M. H., Behannon, K. W., Burlaga, L. F., Connerney, J. E. P., Lepping, R. P., and Neubauer, F. M., "Magnetic Fields at Uranus," *Science*, vol. 233, pp. 85–89, July 4, 1986.

Riddle, A. C., and Warwick, J. W., "Redefinition of system III longitude, *Icarus*, vol. 27, pp. 457–459, 1976.

Seidelmann, P. K., and Divine, T. N., Evaluation of Jupiter longitudes in System III (1965), *Geophys. Res. Lett.*, vol. 4, 65-68, 1977.

Selesnick, R.S., and Stone, E.C., "Energetic electrons at Uranus: Bimodal diffusion in a satellite limited radiation belt," *J. Geophys. Res.*, vol. 96, no. A4, pp. 5651–5665, 1 April 1991.

Smith, B. A., Soderblom, L. A., Beebe, R., Bliss, D., Boyce, J. M., Brahic, A., Briggs, G. A., Brown, R. H., Collins, S. A., Cook II, A. F., Croft, S. K., Cuzzi, J. N., G. E. Danielson, M. E. Davies, T. E. Dowung, D. Godfrey, C. J. Hansen, C. Harris, G. E. Hunt, A. P. Ingersol, T. V. Johnson, R. J. Krauss, H. Marsursky, D. Morrison, T. Owen, J. B. Plescia, J. B. Pollack, C. C. Porco, K. Rages, C. Sagan, E. M. Shoemaker, L. A. Sromovsky, C. Stoker, R. G. Strom, V. E. Suomi, S. P. Synnott, R. J. Terrile, P. Thomas, W. R. Thompson, J. Veverka, "Voyager 2 in the Uranian System: Imaging Science Results," *Science*, vol. 233, pp. 43–64, July 4, I986.

Vision and Voyages for Planetary Science in the Decade 2013-2022, National Academy of Sciences, Washington, D.C., 2011.

14. Appendix A1. Fits To the LEPD and TET Differential Intensity Spectra

Figure A1-1 shows fits to Fig. 10 of Mauk et al. (1987) LECP and Fig. 3 from Selesnick and Stone (1991) for the TET. Note that UMOD is first fit to the Mauk et al. data and then, for the electrons above ~0.5-1 MeV, approximated by the TET electron power law spectrum above that energy range.

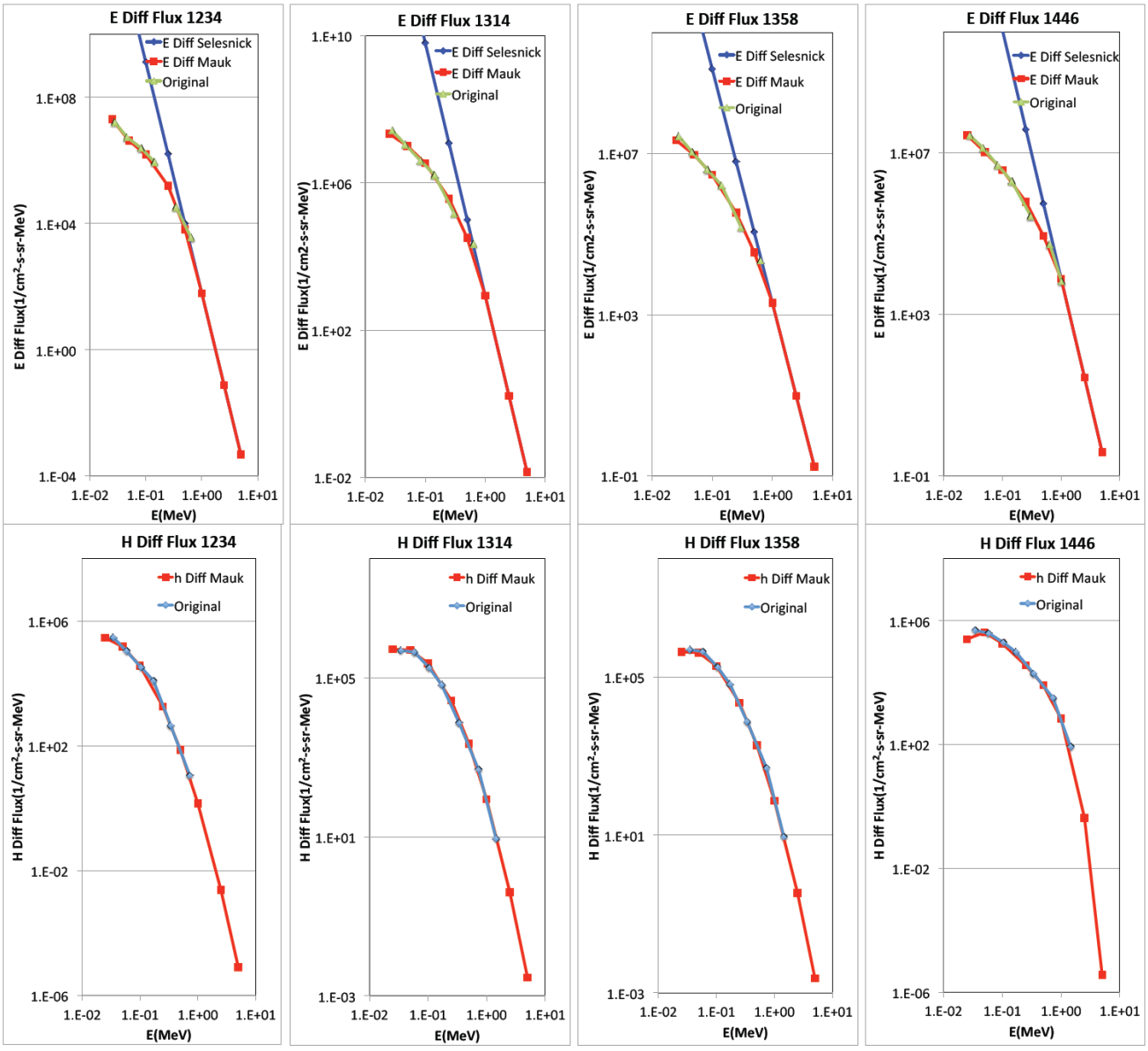

Figure A1-1. Polynomial fits (red) to the original LECP (green) electron and (blue) proton differential intensity spectra and power law fits to the high energy TET (blue) electron differential intensity spectra. The electron spectrum at 13:14 is from Selesnick and Stone whereas the proton spectrum was assumed to be that at 13:58.

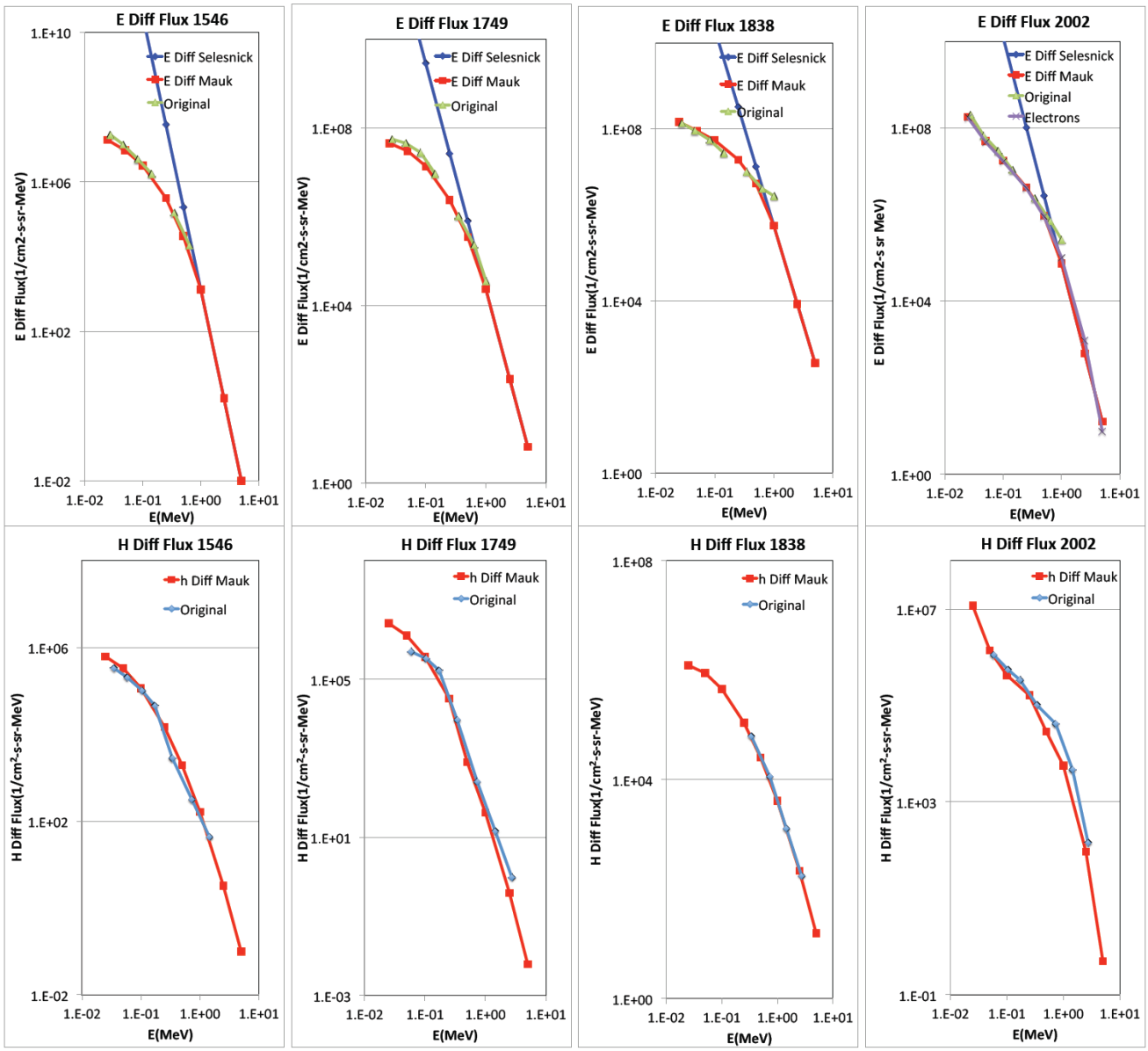

Figure A1-1. Polynomial fits (red) to the original LECP (green) electron and (blue) proton differential intensity spectra and power law fits to the high energy TET (blue) electron differential intensity spectra. The electron spectrum at 13:14 is from Selesnick and Stone whereas the proton spectrum was assumed to be that at 13:58. (Continued)

15. Appendix A2. Acronyms, Abbreviations, and Terms

APL	Johns Hopkins University Applied Physics Laboratory
B	magnetic field at the spacecraft
B-L	magnetic field coordinates of a point
CR	count rate
CRS	Cosmic Ray Subsystem (on Voyager 2)
CTS	counts per second
J2000	international standard for starting time referencing noon, Jan. 1, 2000
JHU	Johns Hopkins University
L	the magnetic L-shell parameter
LECP	Low Energy Charged Particle Detector on Voyager 2
NAIF	(NASA) Navigation and Ancillary Information Facility
NPPA	North Pole Position Angle
OTD	Offset Tilted Dipole magnetic field model
PDS	Planetary Data System
PHA	pulse height analyzer
PHI	east longitude
Q_3	mulit-pole expansion model of Connerney Uranian magnetic field
R^2	regression coefficient
RA	right ascension
RMS, rms	root mean square
R_U	Uranian radius, 21,645 km

SCET Spacecraft Event Time

SIII jovocentric rotating coordinates

SPICE

- Spacecraft ephemeris, given as a function of time. (SPK)
- P- Planet, satellite, comet, or asteroid ephemerides, or more generally, location of any target body, given as a function of time. (also SPK)
- The P kernel also logically includes certain physical, dynamical and cartographic constants for target bodies, such as size and shape specifications, and orientation of the spin axis and prime meridian. (PCK)
- Instrument description kernel, containing descriptive data peculiar to a particular scientific instrument, such as field-of-view size, shape and orientation parameters. (IK)
- C- Pointing kernel, containing a transformation, traditionally called the "C-matrix," which provides time-tagged pointing (orientation) angles for a spacecraft bus or a spacecraft structure upon which science instruments are mounted. A C-kernel may also include angular rate data for that structure. (CK)
- E- Events kernel, summarizing mission activities - both planned and unanticipated. Events data are contained in the SPICE EK file set, which consists of three components: Science Plans, Sequences, and Notes. (EK))

TET "The Electron Telescope" on Voyager 2

TID total ionizing dose

UMOD Uranus Radiation Model

Ul Uranian longitude

UT Universal Time